NAVAL POSTGRADUATE SCHOOL
MONTEREY, CALIFORNIA

THESIS

IN-SITU MEASUREMENT OF TOTAL DOSE RADIATION EFFECTS ON PARALLEL PLATE MOS CAPACITORS USING THE NPS LINEAR ACCELERATOR

by

Stuart M. Abrahamson

December 1995

Thesis Advisors: **Sherif Michael**
Oscar Biblarz

Approved for public release; distribution is unlimited.

REPORT DOCUMENTATION PAGE

Form Approved OMB No. 0704-0188

1. AGENCY USE ONLY *(Leave blank)*	2. REPORT DATE December 1995	3. REPORT TYPE AND DATES COVERED Master's Thesis

4. TITLE AND SUBTITLE IN-SITU MEASUREMENT OF TOTAL DOSE RADIATION EFFECTS ON PARALLEL PLATE MOS CAPACITORS USING THE NPS LINEAR ACCELERATOR	5. FUNDING NUMBERS
6. AUTHOR(S) Abrahamson, Stuart M.	
7. PERFORMING ORGANIZATION NAME(S) AND ADDRESS(ES) Naval Postgraduate School Monterey CA 93943-5000	8. PERFORMING ORGANIZATION REPORT NUMBER
9. SPONSORING/MONITORING AGENCY NAME(S) AND ADDRESS(ES)	10. SPONSORING/MONITORING AGENCY REPORT NUMBER

11. SUPPLEMENTARY NOTES The views expressed in this thesis are those of the author and do not reflect the official policy or position of the Department of Defense or the U.S. Government.

12a. DISTRIBUTION/AVAILABILITY STATEMENT Approved for public release; distribution is unlimited.	12b. DISTRIBUTION CODE

13. ABSTRACT *(maximum 200 words)*

The study of radiation effects to electronics circuits has been ongoing almost as long as there have been satellites and spacecraft in space. The response to radiation over the planned life of the space system is of great concern to system designers. Operational amplifiers are one of the most basic elements in all electronic systems. This research examines radiation effects of part of a Metal Oxide Semiconductor (MOS) operational amplifier and is applicable to Complimentary MOS (CMOS) technology as well. More specifically, it is pertinent to MOS capacitors used to internally compensate op amps. First, a review of semiconductor theory is presented followed by a discussion of damage mechanisms to MOS capacitors and a brief look at operational amplifier fundamentals. MOS capacitors, constructed by previous research efforts using the MOSIS technique, were selected as the internally compensating elements for simple low pass filters. Using the Naval Postgraduate School linear accelerator, these capacitors were irradiated with pulsed electrons possessing energies of up to 26 MeV for varying times. In-situ measurements were taken to immediately determine the capacitance value via the measured filter break frequency as a function of fluence. Separate irradiation runs were performed on three MOSIS capacitors and were terminated upon filter failure. This research concludes with a hypothesis of the filter failure mechanism and suggested areas for expansion of continuing research efforts. This is believed to be the first time such an experiment has been performed.

14. SUBJECT TERMS Simulations, Software Project Management, System Dynamics, User Interfaces,	15. NUMBER OF PAGES 100
	16. PRICE CODE

17. SECURITY CLASSIFICATION OF REPORT Unclassified	18. SECURITY CLASSIFICATION OF THIS PAGE Unclassified	19. SECURITY CLASSIFICATION OF ABSTRACT Unclassified	20. LIMITATION OF ABSTRACT UL

NSN 7540-01-280-5500

Standard Form 298 (Rev. 2-89)

Prescribed by ANSI Std. 239-18 298-102

Approved for public release; distribution is unlimited.

IN-SITU MEASUREMENT OF TOTAL DOSE RADIATION EFFECTS ON PARALLEL PLATE MOS CAPACITORS USING THE NPS LINEAR ACCELERATOR

Stuart M. Abrahamson
Lieutenant, United States Navy
B.S., Northwestern University, 1987

Submitted in partial fulfillment
of the requirements for the degrees of

MASTER OF SCIENCE IN ELECTRICAL ENGINEERING
AND
MASTER OF SCIENCE IN ASTRONAUTICAL ENGINEERING

from the

NAVAL POSTGRADUATE SCHOOL
December 1995

Author: _____
Stuart M. Abrahamson

Approved by: _____
Sherif Michael, Thesis Advisor

_____
Oscar Biblarz, Thesis Advisor

_____
Herschel H. Loomis, Jr., Chairman
Department of Electrical and Computer Engineering

_____
Daniel J. Collins, Chairman
Department of Aeronautical and Astronautical Engineering

ABSTRACT

The study of radiation effects to electronics circuits has been ongoing almost as long as there have been satellites and spacecraft in space. The response to radiation over the planned life of the space system is of great concern to system designers. Operational amplifiers are one of the most basic elements in all electronic systems. This research examines radiation effects of part of a Metal Oxide Semiconductor (MOS) operational amplifier and is applicable to Complimentary MOS (CMOS) technology as well. More specifically, it is pertinent to MOS capacitors used to internally compensate op amps. First, a review of semiconductor theory is presented followed by a discussion of damage mechanisms to MOS capacitors and a brief look at operational amplifier fundamentals. MOS capacitors, constructed by previous research efforts using the MOSIS technique, were selected as the internally compensating elements for simple low pass filters. Using the Naval Postgraduate School linear accelerator, these capacitors were irradiated with pulsed electrons possessing energies of up to 26 MeV for varying times. In-situ measurements were taken to immediately determine the capacitance value via the measured filter break frequency as a function of fluence. Separate irradiation runs were performed on three MOSIS capacitors and were terminated upon filter failure. This research concludes with a hypothesis of the filter failure mechanism and suggested areas for expansion of continuing research efforts. This is believed to be the first time such an experiment has been performed.

TABLE OF CONTENTS

LIST OF FIGURES

ACKNOWLEDGMENTS

There are numerous persons deserving acknowledgment and who are at least partially responsible for the successful completion of this research. First, I would like to thank the double-hatted Dr. Sherif Michael, for not only serving as thesis advisor but also as mentor, offering precious assistance throughout my tour at the Naval Postgraduate School. Next, to Dr. Oscar Biblarz, who graciously and gallantly offered to be my co-advisor. My appreciation is extended to the staff of the Electrical and Computer Engineering Circuits Lab for lessons in experimental circuit construction and measurement. Thanks to the Linear Accelerator staff, as this experiment would not have been possible without their hard work. Also, thanks to the Space Systems Academic Group PANSAT design team both for the construction of the coaxial jack interface and use of their digital camera used to take a plethora of action shots in the LINAC. Finally, thanks to my wife, Cathy, as her infinite amount of patience, understanding and devotion are paramount to our success.

I. INTRODUCTION

With the advent of the information age, satellites are increasingly deployed into diverse orbits for missions such as communication, navigation, weather forecasting, mapping terrain, remote sensing, and interplanetary exploration, just to name a few. Mankind has just begun to realize the profits of space exploration. The operational amplifier, also known as the op amp, is a basic building block for electronic circuits. Every spacecraft contains numerous applications of the op amp. Examples include active and switched capacitor filters, A/D and D/A converters, level shifters, decoders and buffers just to name a few.

The space age began approximately one half century ago when scientists began using remaining rockets from World War II to physically measure the Earth's upper atmosphere. In July, 1955, the U.S. announced it would launch unmanned Earth-circling satellites. Shortly following this declaration, the Soviet Union announced similar intentions and on October 4, 1957, the small satellite Sputnik was launched from the Soviet Union. The United States followed suit shortly thereafter with the successful launch of Explorer I and the great Space Race began. [Ref. 1, p. 2.1-1]

In the quest to understand the near-Earth space environment, several exoatmospheric nuclear tests as listed in Table 1.1 were conducted. The four latter nuclear detonations produced significant disruption of the radiation belts, discussed in Chapter II, to cause an orbiting communications satellite, Telstar I, to completely fail. Immediately following this failure, then Soviet Union Premier, Nikita Khruschchev,

announced "such radiation vulnerability would be considered a possible means to destroy future U. S. military space systems." [Ref. 1, p. 2.1-2] These words quickly escalated United States research efforts to understand both the natural and man-made space radiation environment and apply that knowledge toward protecting future satellite systems.

Explosion	Location	Date	Yield (kt)	Altitude (km)
Argus I	South Atlantic	27 August 1958	1	200
Argus II	South Atlantic	30 August 1958	1	250
Argus III	South Atlantic	09 September 1958	1	500
Starfish	Johnson Island, Pacific Ocean	09 July 1962	1400	400
USSR	Siberia	22 October 1962	Hundreds	Unknown
USSR	Siberia	28 October 1962	≈1000	Unknown
USSR	Siberia	01 November 1962	1000	Unknown

Table 1. 1 Known exoatmospheric nuclear tests. From [Ref. 1, p. 2.1-2]

Currently, there appear to be no man-made threats to satellite systems. However, the natural radiation environment continues to be quite a viable threat to space-borne electronic systems. The circuit designer must be cognizant of radiation threats to his or her system and must take steps to insure performance to specifications for the duration of the designed system life. He or she must be aware of the spacecraft orbit parameters such as altitude, inclination and eccentricity, since the radiation environment is both position and time dependent.

The study of radiation damage to electronics is a large field which has blossomed since the Starfish incident in Table 1.1. A tremendous amount of effort has been expended to describe and understand the mechanisms between radiation and materials

and more specifically, semiconductor materials and the effects of radiation on electronic systems. The primary emphasis of this work is to examine, in-situ, the total dose effects of damaging radiation on metal-oxide-silicon (MOS) capacitors utilizing a beam of pulsed electrons originating from a linear accelerator.

This thesis starts off with a discussion of the natural space radiation environment including trapped particles found in typical orbits. Next, a review of semiconductor physics in Chapter III followed by a narrowed scope which examines MOS capacitor fundamentals in Chapter IV. MOS capacitor radiation damage mechanisms are considered in Chapter V. The formation and procedure of the experiment are found in Chapter VI and Chapter VII, respectively. Results and recommendations conclude this study in Chapter VIII.

II. THE NATURAL SPACE RADIATION ENVIRONMENT

A. AN HISTORICAL OVERVIEW

The space age, by most accounts, was born in 1946 when scientists began using rockets left over from World War II to take measurements of the Earth's upper atmosphere. Prior to this time, little was known of the space environment as a whole, let alone the complex radiation environment which embodies the Earth. The following was the conventional wisdom of the time: [Ref.1, p.2.1-1]

- The Earth's atmosphere was thought to extend upward a few hundred miles then essentially end
- The Earth's magnetic field, as shown in Figure 2.1, was thought to be similar to a bar magnet, extending into space and gradually getting weaker and weaker
- The Sun was thought to emit little but visible light
- It was understood that a magnetic storm frequently occurred at the Earth shortly after a solar flare

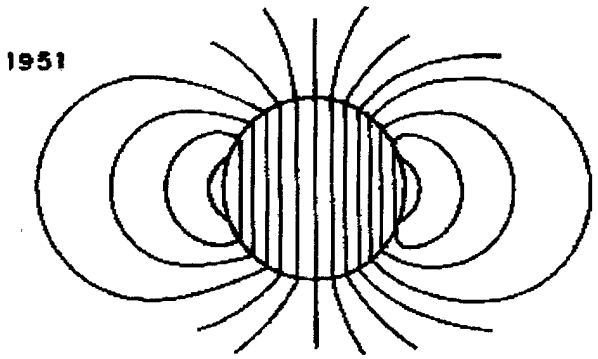

Figure 2. 1 Early theory of Earth's magnetic field. From Ref. [2, p. 4-2]

The first attempt at mapping the radiation environment came with the launch of the Explorer I satellite in January, 1958. It carried onboard a geiger counter supplied by Professor Van Allen from Iowa University. Since this satellite had no onboard data

storage capability, it could only provide limited counter readings while within transmission range of a ground station. Post-flight analysis of these data revealed gaps in cosmic rays at high altitudes over South America. The Explorer II mission failed, so it was not until the successful launch of Explorer III, with an onboard recording device, that an area of extremely high particle flux, later named the South American Anomaly (SAA), was first detected.

After the discovery of the SAA, more spacecraft were launched. Pioneer III, intended to become a lunar probe reaching a peak altitude of only 107,400 km, but could not break free of the gravitational pull of the Earth. Armed with 2 geiger counters and recording counts per unit time during the orbit, Pioneer III was able to more completely measure the extent of trapped radiation previously detected by Explorer I. By combining data from Pioneer III and Explorer IV, Van Allen, et al, were able to construct "the first complete map of trapped radiation and to the concept of inner zones and outer zones as we understand them today" [Ref.1, p.2.1-2]. This map is shown in Figure 2.2.

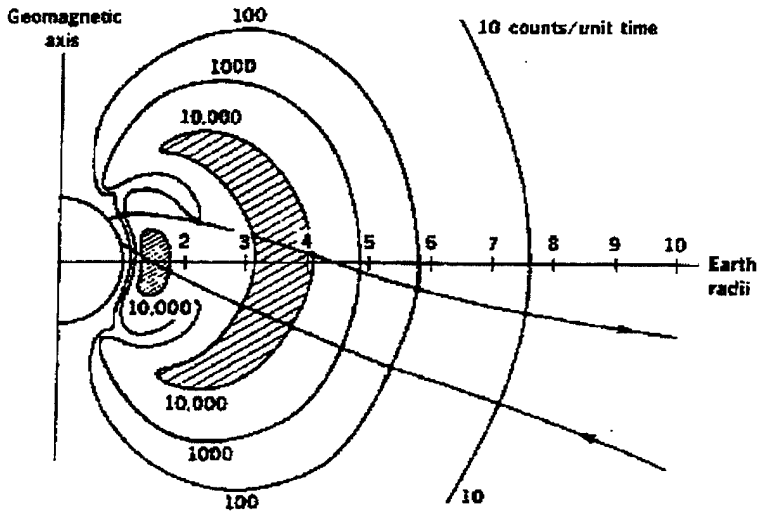

Figure 2. 2 Van Allen's map of the radiation belts. From Ref. [3, p. 39]

Since the discovery of these Van Allen belts, knowledge of the radiation particles in the Earth's geomagnetic field and other damaging elements in the space radiation environment has drastically increased. The next section takes a closer look at the particles in this environment.

B. PARTICLES OF THE NATURAL SPACE ENVIRONMENT

There are two classifications for particles in the natural space environment. The first class characterizes particles trapped in the Earth's magnetic field while the other describes particles of solar or galactic origin called cosmic rays.

1. Trapped Particles

The Earth is encased in a nonuniform enclosure called the magnetosphere, which consists of magnetic field lines and charged particles which become trapped by the magnetic field. This is shown in Figure 2.3. The magnetosphere is hemispherical on the day side, extending out to approximately 10 $R_{\oplus}$. Recall the radius of Earth, $R_{\oplus}$, is 6378 km. On the night side, it is an extremely long cylinder (hundreds of earth radii) due to the solar wind, with an approximate diameter of 40 $R_{\oplus}$. The area of interest for particle trapping, where the majority of earth bound satellites reside, is the relatively small region labeled plasmasphere.

Typically, relatively lower energy protons and electrons become trapped, but some heavy ions manage to become captured as well. The trapped particles gyrate spirally around the magnetic field lines and are reflected back and forth between the poles where the field is confined [Ref.5, p. II-4]. This motion is illustrated in Figure 2.4. The particles also drift around the Earth, electrons to the east and protons to the west. The

totality of these gyrating, bouncing and precessing protons and electrons (and other ions) constitute the Van Allen radiation belts [Ref.2, p. 5-9]. Table 2.1 shows the characteristic time scales for a typical 1MeV particle at with an altitude of 2000 km.

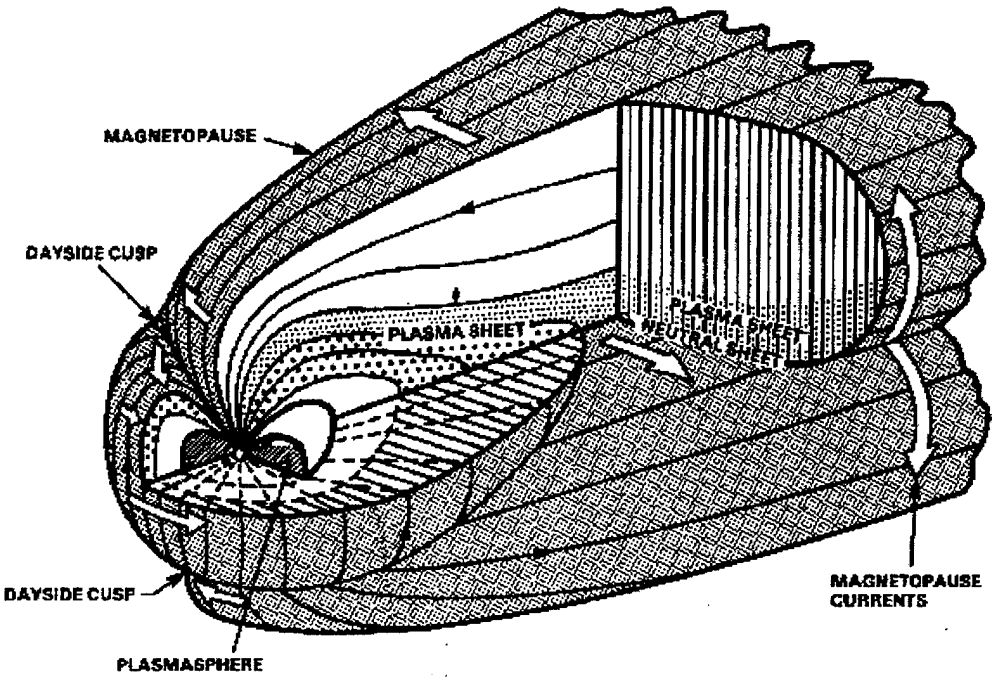

Figure 2. 3 The Magnetosphere. From Ref. [4, p. 1424]

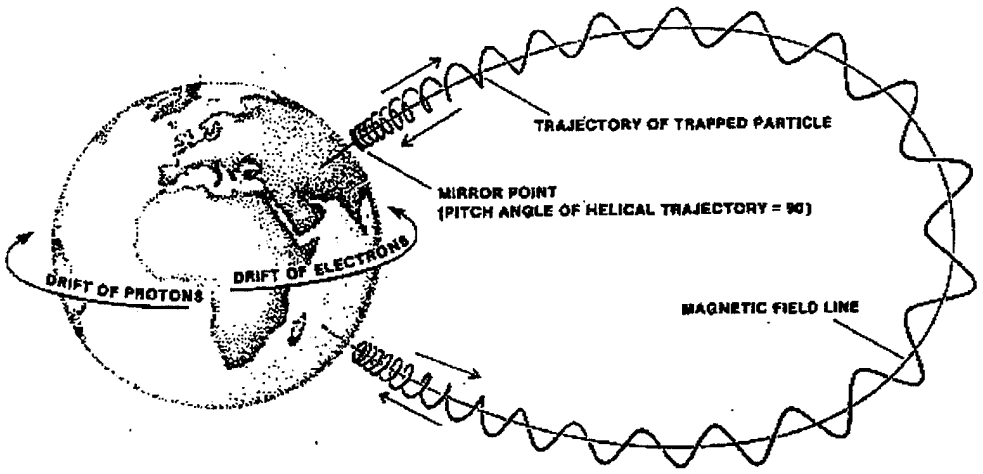

Figure 2. 4 Trapped particle motion. From Ref. [4, p. 1425]

	Electrons	Protons
Gyration Period	7.0×10^{-6} seconds	4.0×10^{-3} seconds
Bounce Period	0.1 seconds	2.2 seconds
Drift Period	53 minutes	32 minutes

Table 2. 1 Characteristic particle motion time From Ref. [2, p. 5-10]

Before proceeding any further, definitions for flux and fluence are discussed. Flux is the *rate* at which particles impinge upon a unit surface area, given by units of particles/cm^2-s. Fluence is the integral over time of flux. Thus, fluence is equal to the *total number* of particles which impinge upon a unit surface area over a specified time and has units of particles/cm^2.

The location of the orbit within the magnetosphere will determine dominate types of particles the spacecraft will encounter. The magnetosphere can be partitioned into five regions which, as discussed below, have complex constantly moving boundaries that are only guidelines at best. A label for determining a unique position in the radiation belts, called the L-Value, was developed by Carl McIlwain. [Ref. 2, p. 5-11] The L-value for a given magnetic field line is found using equation 2.1.

$$L = \frac{R}{\cos(\lambda_m)^2} \qquad \textbf{(2. 1)}$$

where

R = distance from the center of the earth

λ_m= magnetic latitude in degrees

This L-value, along with a local time, uniquely determine a location within the magnetosphere. It should be noted, however, the McIlwain number becomes increasingly inaccurate at altitudes greater than geosynchronous ($\approx$6.6 $R_\oplus$) due to the magnetic field

complexities discussed in section C of this chapter. The types of particles and their areas of dominance are depicted in Figure 2.5. [Ref. 2, p. 5-11] [Ref. 4, p. 1424]

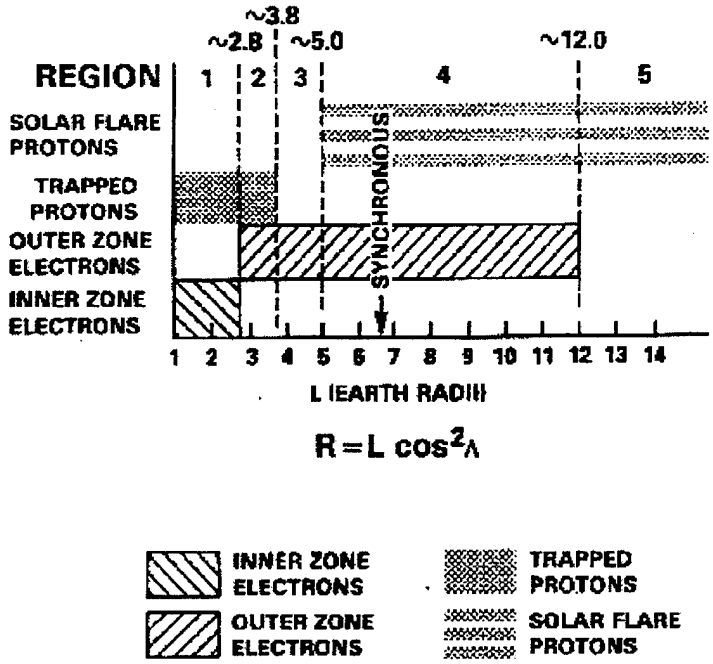

Figure 2. 5 Magnetosphere charged particle distribution. From [Ref. 4, p. 1425]

a. Electrons

Electrons found in the Van Allen belts are divided between inner and outer zones. The inner zone extends to approximately 2.5 $R_{\oplus}$ and the outer zone stretches to 12 $R_{\oplus}$. The area between 2.5 $R_{\oplus}$ and 2.8 $R_{\oplus}$ is known as the slot. Electron density is typically low during times of infrequent magnetic storms but can increase several orders of magnitude as storm activity grows. Accepted values for the energy of these trapped electrons are < 5 MeV and ≈7 MeV for the inner and outer zones, respectively. It is interesting to note that the flux for outer zone electrons is normally ten times that of the inner zone species. Also, the peak flux location for electrons with a minimum energy of

1 MeV is found between 3 and 4 $R_{\oplus}$. Electron interactions must be considered for total dose effects to circuits but may be dismissed for single-event upsets. [Ref. 5, p. II-5]

b. Protons

Trapped protons exist primarily in regions 1 and 2 up to an altitude of ≈3.8 $R_{\oplus}$ with peak energies of 500 MeV. Note that typical spacecraft shielding can attenuate protons with energies less than 10 MeV. Figure 2.6 shows how protons with specific energy levels vary with altitude. Thus, it is shown that above 3.8 $R_{\oplus}$, trapped protons are of little concern for radiation damage. However, there exist high energy protons with peak fluxes at about 1.6 earth radii. [Ref. 5, p. II-5]

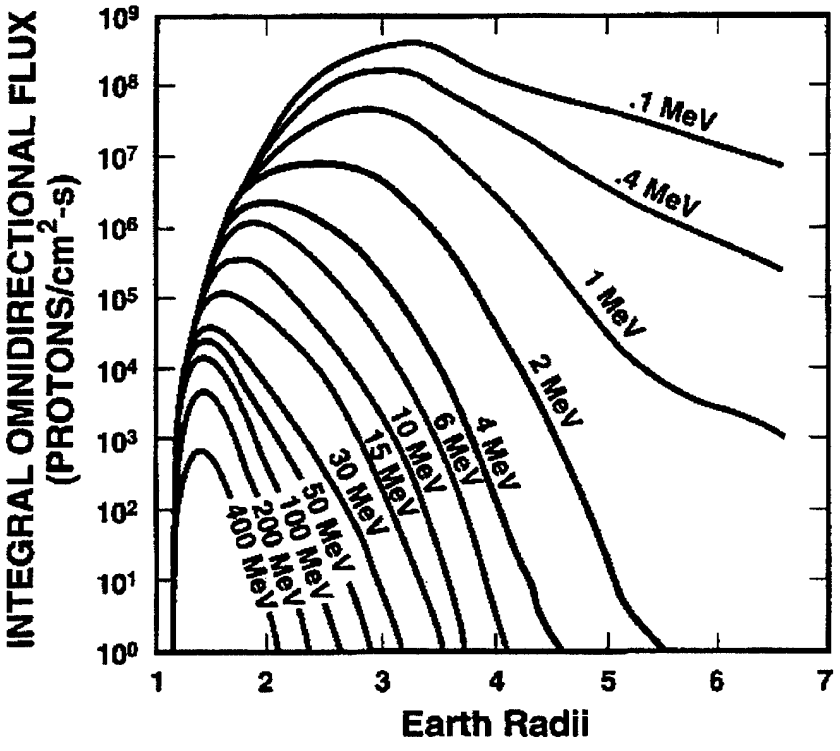

Figure 2. 6 Proton flux as a function of altitude and energy. From [Ref. 4, p. 1426]

There is a region in a LEO orbit where flux for protons with energies greater than 30 MeV can be up to 4 orders of magnitude higher than anywhere else in the orbit. "This is primarily the result of the offset of the dipole term of the geomagnetic field by approximately 11° from the earth's axis of rotation and displacement of about 500 km toward the Western Pacific. The effect is an apparent depression of the magnetic field over the coast of Brazil." [Ref. 4, p. 1424] The previously mentioned South American Anomaly (SAA), initially discovered by Van Allen, et al, is responsible for the majority of trapped radiation received by a spacecraft in LEO. Interestingly enough, on the opposite side of the magnetic depression is the Southeast-Asian Anomaly, the trapped particle belts are located at a higher altitude and are not responsible for significant amounts of radiation exposure.

2. Cosmic Rays

Cosmic rays were first discovered by Victor Hess, an Austrian physicist, in 1911. There are two known sources of cosmic rays. They are either galactic (originating outside our solar system) or solar (originating from the sun). It is currently believed that the galactic spectrum outside our solar system is fairly uniform while solar cosmic rays occur randomly.

a. Galactic Cosmic Rays

The vast majority of cosmic rays emanate from outside our solar system in the Milky Way and even beyond where the sources are not well understood. They are composed of mostly protons (85%) and alpha particles or helium nuclei (14%). The

remainder of the spectrum is composed of electrons, gamma rays and high energy heavy ions. The small percentage of heavy ions does not equate to small radiation effects, rather, heavy ions deposit more energy per unit depth than protons. Figure 2.7 illustrates the energy spectrum of galactic cosmic rays. Expected energy ranges for protons and alpha particles can be more than 100 GeV/nucleon. It can be clearly seen that the peak fluxes occur for most ions with energies in the 0.1 to 1 GeV/nucleon range. It is nearly impossible to shield spacecraft electronics from these high energy particles. [Ref. 6, p. 461] [Ref. 5, p. II-6-7]

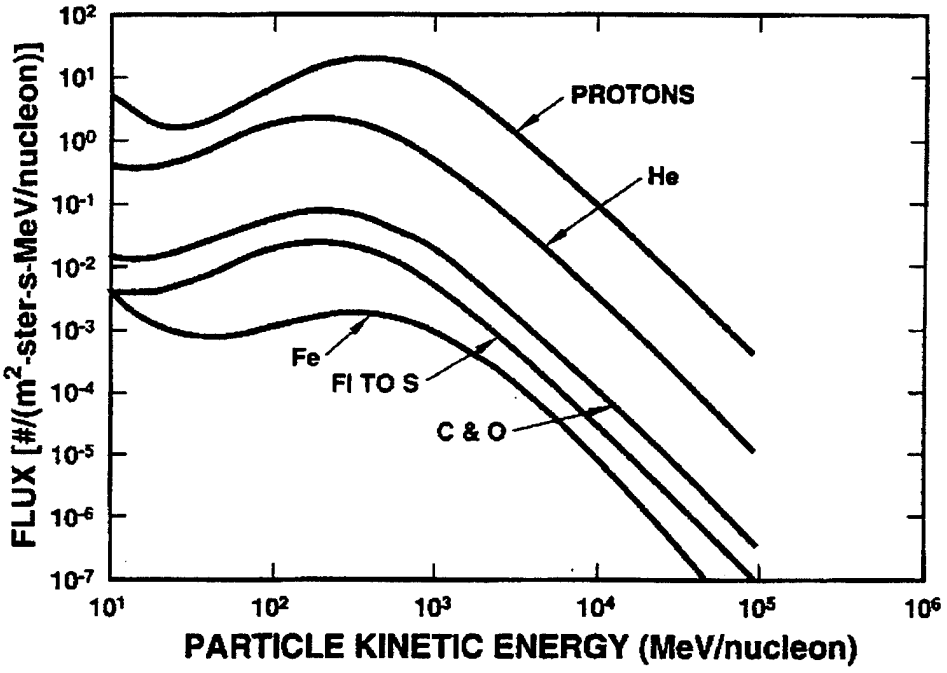

Figure 2. 7 Energy spectrum of galactic cosmic rays. After [Ref. 7]

b. Solar Cosmic Rays

Solar flares are generally responsible for solar cosmic rays and are tied to the solar activity cycle, which is 22 years in duration. Independent solar flares are

unpredictable in nature but generally increase and decrease with a period of 11 years. It takes a complete reversal in the suns magnetic field, or 2 solar flare activity periods to complete the solar activity cycle. [Ref. 2, p. 2-17]

After a solar flare occurs, particles begin to arrive near the earth within 10 minutes, peak in intensity within two hours to one day and, except for a few particles which become trapped in the magnetosphere, are gone within a few days to a week. Solar cosmic rays consist mainly of protons and alpha particles with a very small percentage being heavy ions. This heavy ion concentration can be neglected when compared to the concentration of cosmic heavy ions. However, the amount of protons and alpha particles originating from the sun can be up to 10,000 times the amount found in the galaxy outside our solar system. Clearly, they are not to be neglected. [Ref. 5, p. II-8]

Accompanying the solar flare is a plasma known as the solar wind. By definition, a plasma contains equal amounts of charged particles and, thus, is electrically neutral. But as the "solar wind strikes the magnetosphere, it can cause disturbances in the geomagnetic fields...compressing them towards the earth. As a result, the solar wind can enhance the total dose that a spacecraft in LEO can receive." [Ref. 2, p. II-8] Refer to Figure 2.8.

C. MODELING OF THE RADIATION ENVIRONMENT

Accurately modeling the magnetosphere so that one may predict and adequately design for expected radiation exposure to satellite electronic systems is a daunting task, to say the least. The job is complicated for various reasons as the magnetosphere's composition is a function of many variables. Internal and external magnetic fields are

superimposed upon each other to comprise the total magnetosphere field. The internal field is thought to be caused by convective motion in the molten nickel-iron core of the earth and by residual permanent magnetism in the earth's crust. This field gradually changes over time as the earth's dipole moment shrinks in value and both magnetic pole locations drift. The external field is made of the relatively faster moving currents and fields set up in the magnetosphere by the solar wind. Perturbations due to cyclic variations such as diurnal effects (daily), tilt effects (season), and solar wind (11 year cycle) conditions, as shown in Figure 2.8 and Figure 2.9, all combine to affect the outer magnetosphere, which in turn, modify local field values. [Ref.4, p. 1424]

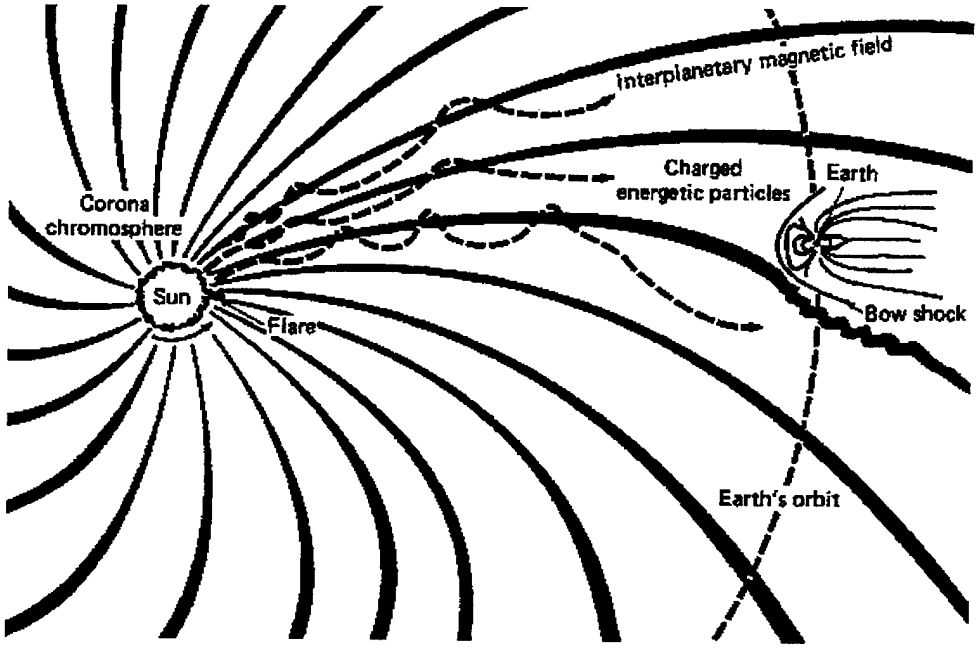

Figure 2. 8 Magnetosphere interaction with solar wind. From Ref. [8, p. 662]

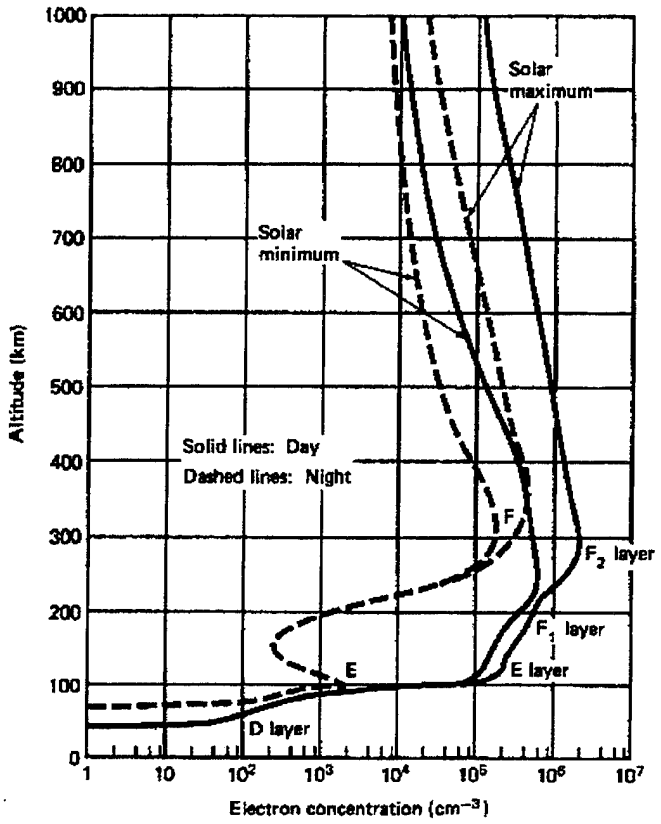

Figure 2. 9 Electron concentration in lower Van Allen belt. © 1971 by Lockheed Missile Systems Division. From Ref. [8, p. 663]

The U.S. National Space Science Flight Data Center (NSSDC) at NASA's Goddard Space Flight Center (GSFC) has developed models to predict the long term average of trapped particle fluxes for any orbit during either solar minimum or maximum. The latest models are AP8 and AE8 for protons and electrons, respectively. Table 2.2 shows a typical prediction of solar minimum proton flux for two circular Low Earth Orbits (LEO) with varying inclination angles.

E(>MEV)	300 KM INCLINATION			500 KM INCLINATION		
	28.5 DEG	60 DEG	90 DEG	28.5 DEG	60 DEG	90 DEG
0.04	2.973E+08	3.203E+09	2.971E+09	5.153E+09	9.171E+09	7.876E+09
0.07	2.351E+08	2.391E+09	2.257E+09	4.082E+09	7.007E+09	6.066E+09
0.10	1.861E+08	1.795E+09	1.730E+09	3.236E+09	5.382E+09	4.712E+09
0.20	5.629E+07	6.779E+08	7.424E+08	9.975E+08	1.908E+09	1.816E+09
0.30	2.227E+07	3.631E+08	4.262E+08	3.969E+08	9.484E+08	9.514E+08
0.40	1.144E+07	2.384E+08	2.849E+08	2.017E+08	5.895E+08	6.029E+08
0.50	5.897E+06	1.616E+08	1.950E+08	1.030E+08	3.807E+08	3.944E+08
0.60	3.985E+06	1.283E+08	1.526E+08	6.850E+07	2.917E+08	3.007E+08
0.70	2.701E+06	1.027E+08	1.204E+08	4.574E+07	2.258E+08	2.315E+08
0.80	1.948E+06	8.399E+07	9.744E+07	3.268E+07	1.813E+08	1.845E+08
0.90	1.494E+06	7.001E+07	8.051E+07	2.494E+07	1.504E+08	1.515E+08
1.00	1.147E+06	5.850E+07	6.669E+07	1.904E+07	1.252E+08	1.248E+08
1.25	7.213E+05	3.857E+07	4.262E+07	1.179E+07	8.119E+07	7.931E+07
1.50	4.549E+05	2.554E+07	2.742E+07	7.310E+06	5.292E+07	5.076E+07
1.75	3.051E+05	1.747E+07	1.828E+07	4.870E+06	3.561E+07	3.371E+07
2.00	2.053E+05	1.199E+07	1.224E+07	3.250E+06	2.407E+07	2.250E+07
2.25	1.392E+05	8.275E+06	8.289E+06	2.194E+06	1.644E+07	1.516E+07
2.50	9.419E+04	5.725E+06	5.637E+06	1.484E+06	1.127E+07	1.026E+07
2.75	3.788E+04	3.899E+06	3.751E+06	5.934E+05	7.373E+06	6.610E+06
3.00	1.521E+04	2.695E+06	2.529E+06	2.405E+05	4.956E+06	4.381E+06
3.25	4.850E+03	1.858E+06	1.695E+06	7.591E+04	3.324E+06	2.862E+06
3.50	1.357E+03	1.292E+06	1.148E+06	2.394E+04	2.274E+06	1.914E+06
3.75	3.874E+02	8.495E+05	7.316E+05	7.263E+03	1.474E+06	1.206E+06
4.00	0.000E+00	5.650E+05	4.726E+05	8.860E+02	9.693E+05	7.712E+05
4.50	0.000E+00	2.066E+05	1.643E+05	0.000E+00	3.493E+05	2.633E+05
5.00	0.000E+00	6.828E+04	5.129E+04	0.000E+00	1.143E+05	7.979E+04
5.50	0.000E+00	1.572E+04	1.188E+04	0.000E+00	2.659E+04	1.751E+04
6.00	0.000E+00	2.858E+03	1.970E+03	0.000E+00	3.923E+03	2.470E+03
6.50	0.000E+00	0.000E+00	0.000E+00	0.000E+00	1.235E+02	6.052E+01
7.00	0.000E+00	0.000E+00	0.000E+00	0.000E+00	0.000E+00	0.000E+00

Table 2. 2 Trapped proton fluxes, LEO, Solar Minimum. From Ref. [9]

III. SEMICONDUCTOR REVIEW

A. SILICON

In the early 1950's, germanium, an element found in column IV of the periodic table, was the most extensively used semiconductor material. However, it was found to have high leakage currents at only slightly elevated temperatures. Approximately a decade later, silicon, also in column IV, replaced germanium as the most widely used semiconductor element. The advantages literally abound as silicon, in the form of silica and silicates, comprise 25% of the Earth's crust, is second only to oxygen in abundance and is very inexpensive. In addition to its copiousness, silicon exhibits much lower leakage currents and a high quality oxide layer, that has an excellent insulating property, can easily be produced. Other types of semiconductors which are composed of multiple elements, such as gallium arsenide exist, but will not be examined here. [Ref. 10, p. 3]

1. Energy Bands

Silicon atoms are arranged in a diamond lattice structure. This means all atoms are identical and are surrounded by four equidistant atoms positioned at the corners of a tetrahedron. Each atom has four electrons, called valence electrons, which are shared with the four neighboring atoms. These shared bonds are referred to as covalent bonds. At lower temperatures, the electrons are bound to their respective tetrahedron lattice and are not available for conduction. As the temperature increases, thermal vibrations can break the covalent bonds, resulting in an electron and a hole. See Figure 3.1. Another adjoining electron can fill this hole and in the process, create a hole at a new position.

Thus, under the force of an applied electric field, these electrons and holes move in opposite directions and give the appearance of a current.

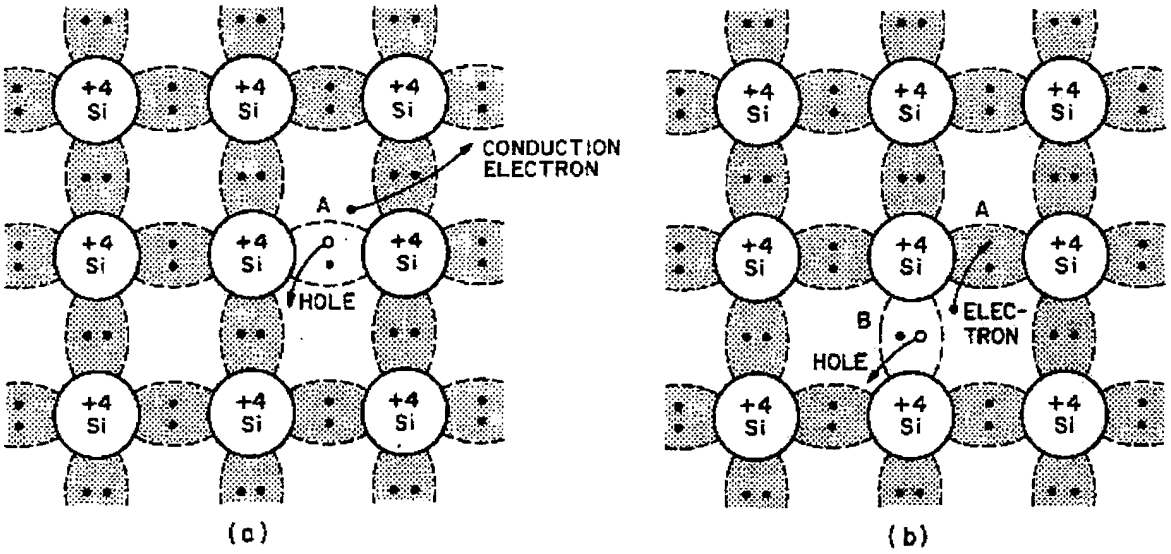

Figure 3. 1 (a) A broken bond at position A, resulting in a conduction electron and a hole. (b) A broken bond at position B. After [Ref. 10, p. 9]

According to the Bohr model, electrons of a single atom can have only discrete energy levels. However, inside a lattice and within a maximum value for lattice spacing, there exist two permitted and one excluded regions. For silicon, when the lattice constant is $\leq 5.43 \times 10^{-10}$ m, electrons can reside either in the conduction or valence band. The region between the two bands is referred to as the forbidden gap and as the name suggests, electron residence is not permitted here. Figure 3.2a shows the relationship between conduction band energy (E_c), valence band energy (E_v) and the forbidden gap. The bandgap energy (E_g) is 1.12 eV for silicon at room temperature and normal atmospheric pressure. This value varies with temperature by

$$E_g(T) = 1.17 - \frac{(4.73 \times 10^{-4})T^2}{(T + 636)} \quad \text{for silicon} \qquad \textbf{(3. 1)}$$

where

E_g = bandgap energy in eV
T = temperature in Kelvin

According to quantum theory, electrons and holes must obey the relationship given by the Fermi-Dirac distribution function. It then becomes necessary to determine two values for semiconductor holes and electrons. The first is energy state occupation probability and the second is the number density of electron and hole states. [Ref. 10, p. 8-15][Ref. 8, p. 9]

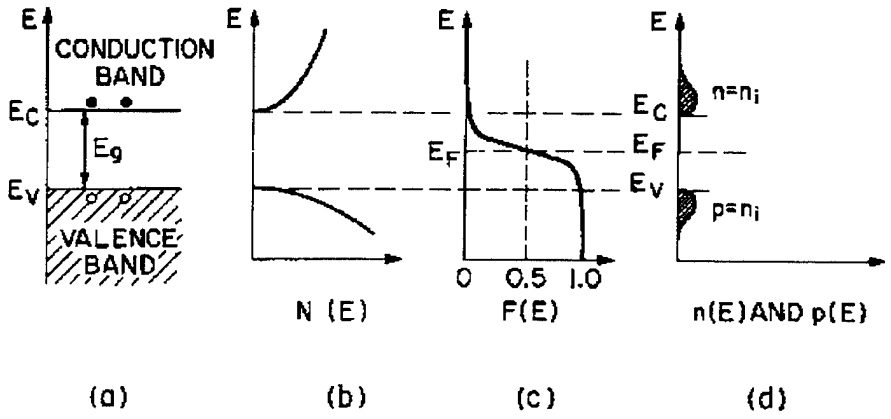

Figure 3. 2 Intrinsic silicon. (a) Band diagram. (b) Density of states (c) Fermi distribution function (d) Carrier concentration. From [Ref. 10, p. 18]

The probability that an electron with energy E is occupying a specific energy state is given by

$$f(E) = \frac{1}{1 + \exp(E - E_f / kT)} \qquad \textbf{(3. 2)}$$

where

E = energy state, eV
k = 8.63×10^{-5} eV/K, Boltzmann's constant
T = temperature, K
E_f = Fermi energy level

It can easily be seen when E=E_f, $f(E) = ½$. The Fermi level is the energy at which the probability of occupation by an electron in thermal equilibrium is exactly one half [Ref. 10, p. 16].

2. Intrinsic Silicon

To determine the second qualitative variable, the number density of electron or hole states $N_{e,h}(E)$, quantum mechanics is once again employed. The number density of states, or the density of allowable states per unit volume, is the distribution of available states for an electron to occupy near the bottom of the conduction band. It is given by

$$N_e(E) = M\frac{\sqrt{2(E-E_c)}(m_{de}^*)^{3/2}}{\pi^2 h^3} \quad \text{for } E \geq E_c \qquad \textbf{(3. 3)}$$

where

M = number of conduction band minima in the energy momentum reciprocal lattice space. M is often included in m_{de}.

m_{de}^* = density of states effective mass for electrons

E_c = energy at the bottom of conduction band, eV

The actual density of electrons of a given energy can now be derived as simply the product of the number of states available in the conduction band multiplied by the probability of the electron with a particular energy state. Namely, conduction electron density is

$$n_o = \int_{Ec}^{\infty} N_e(E) f(E) dE \qquad \textbf{(3. 4)}$$

where the upper limit of the integral is the top of the conduction band but, due to the "severe cutoff property of $f(E)$, n_o depends weakly on the upper limit and infinity can

be taken for convenience." [Ref. 8, p.12] For the normal cases where $E_c - E_f >> 3kT$, the resulting equation for electron density becomes

$$n_o = N_c \exp(E_f - E_c)/kT, \;\; N_c = 2(2\pi m_{de}^* kT / h^2)^{3/2} \qquad \textbf{(3. 5)}$$

For holes with energy E in the valence band, the number density is $N_h(E)(1-f(E))$. Since a hole is simply the lack of an electron, the probability of an electron occupancy subtracted from one gives the probability of a hole occupancy. The resulting equation for valence band hole density when $E_f - E_v >> 3kT$ is

$$p_o = \int_{-\infty}^{E_v} N_h(E)(1-f(E))dE \qquad \textbf{(3. 6)}$$

Equation 3.6 evaluates to

$$p_o = N_v \exp(E_v - E_f)/kT, \;\; N_v = 2(2\pi m_{dh}^* kT / h^2)^{3/2} \qquad \textbf{(3. 7)}$$

A detailed description of the effective masses (m_{de}^*, m_{dh}^*) is supplied in [Ref. 8, p. 9-11]. Essentially, the mass of the electron (or hole) is compensated by the fact that it experiences forces from both an external field as well as forces from colattice particles. The effective mass is also energy band dependent. [Ref. 8, p. 9-11]

The only carriers present so far are due solely to thermal excitement of the lattice and displacement of electrons across the forbidden gap into the conduction band, which leaves holes in the valence band. Thus, silicon carrier densities are equal and their product is dependent on only temperature. This product

$$n_i^2 = n_o p_o = N_c N_v \exp(E_v - E_c/kT) = N_c N_v \exp(-E_g/kT) \qquad \textbf{(3. 8)}$$

is called the intrinsic carrier density. Equation 3.8 is known as the law of mass action. For silicon at 300 K, $n_i \cong 1.45 \times 10^{10}$ carriers/cm^3. [Ref. 8, p. 13] [Ref. 10, p. 20]

3. Extrinsic Silicon

The intrinsic carrier density is not nearly high enough for correct semiconductor operation. Therefore, impurities must be introduced into the lattice to raise the density using a procedure called doping. Intrinsic silicon atoms are arranged in the lattice to give a density of $\approx 5 \times 10^{22}$ atoms/cm^3. Depending on the level of doping required for the application, the carrier density can be increased by a factor of between 100 and 10 billion times intrinsic amounts. [Ref. 8, p. 15]

The type of excess carrier created can be chosen by the selection of either group III or group V elements used as dopants. If for example, phosphorous, a group V element with five outer shell electrons is used, four electrons are used for covalent bonding with the silicon lattice while the fifth ends up as a free electron available for conduction. However, if a group III element such as boron, with three outer shell electrons is used, a shortage of electrons and consequently an excess of holes will result. Therefore, it is easily seen why group V elements, which donate an electron, are called donors and the corresponding semiconductor is called n-type. Here, electrons are referred to as the majority carriers while holes are minority carriers. Conversely, group III elements are called acceptors and produce p-type semiconductors when introduced into the silicon lattice. As to be expected, the opposite definitions for p-type majority (holes) and minority (electrons) carriers hold true.

Additional energy states are added to the semiconductor with the introduction of these impurities. It turns out that at room temperature, the energy $E = kT = 0.026eV$,

which is adequate energy to ionize the majority of impurity atoms. The vast majority of carriers are a result of impurity ionization and not intrinsically generated. These new additions result in a shift of the Fermi level depending on the type dopant to ensure overall charge neutrality according to Equation 3.9.

$$n + N_A = p + N_D \tag{3.9}$$

where

N_A = acceptor ion density
N_D = donor ion density

For a n-type semiconductor, $N_A << N_D$, which simplifies Equation 3.9. Combining this simplification with Equation 3.5 gives

$$n \approx N_D = N_C \exp((E_f - E_c)/kT) \tag{3.10}$$

which can be rearranged to give

$$E_f = E_C - kT \ln(N_C/N_D) \tag{3.11}$$

So as the number of donor ions converge on N_C, E_f will shift toward E_C. A similar conclusion can be drawn for p-type semiconductors demonstrating the shift in the Fermi level toward the valence band. Figure 3.3 summarizes the preceding discussion. Carrier densities, the Fermi distribution and energy bands for intrinsic and both n and p-type extrinsic semiconductor material are shown. [Ref. 8, p. 16-17] [Ref. 10, p. 22-26]

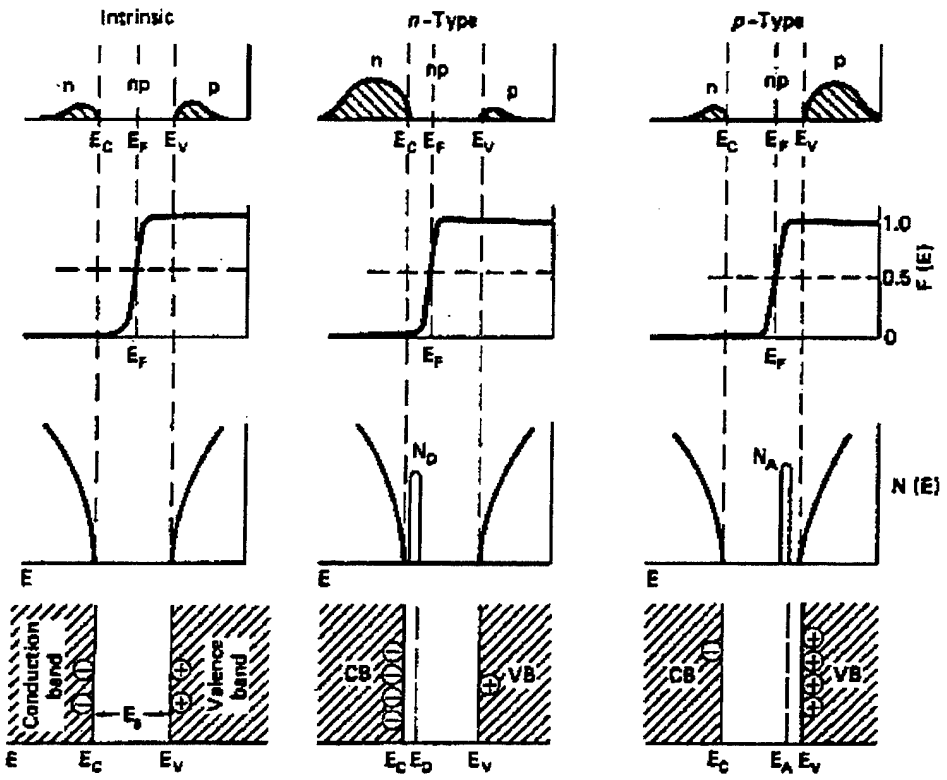

Figure 3. 3 Summary of intrinsic and extrinsic carrier densities, Fermi distribution and energy bands. From [Ref. 8, p. 16]

B. THE P-N JUNCTION

One method of making a useful semiconductor device such as a transistor or diode is to join p-type and n-type semiconductor material together. This joining forms a junction which may be either abrupt or a graded variant, depending on whether the dopant concentrations in the materials gradually match each other or rapidly change at the junction. This research examines the abrupt junction case only. The law of mass action discussed earlier still applies. That is, the product of majority and minority carrier concentrations on either side of the junction equals a constant which is the square of the intrinsic carrier concentration.

1. The Unbiased Depletion Region

The p-n junction is formed using processes such as ion implantation, diffusion and epitaxy. [Ref. 10, p. 71] As the two materials are joined, large carrier concentration gradients exist forcing rapid carrier diffusion. Electrons diffuse from the n to the p-side while holes diffuse from the p to the n-side. Near the junction, this diffusion process leaves positive donor ions on the n-side and negative acceptor ions on the p-side uncovered. This region on either side of the junction is called the space charge or depletion region, due to the lack of mobile carriers. These immobile uncovered ions create an electric field which now opposes further carrier diffusion. Applying the conservation of charge principle and assuming that all donor and acceptor atoms are ionized (a good assumption for room temperature), the electrostatic potential built by the two regions, ϕ_o, is

$$\phi_o = (kT/q)\ln(N_D N_A / n_i^2) \qquad \textbf{(3. 12)}$$

where

N_A = acceptor ion density
N_D = donor ion density
n_i = intrinsic carrier density

At thermal equilibrium, the net current flow across the junction without any external excitations, i.e., no biasing voltages, will be zero. This condition of no current also restricts the Fermi energy level from changing across the junction. On one hand, it must lie close to the *conduction* band on the n-side to accurately reflect the addition of electrons from the n-type donor atoms. On the other hand, it must reflect the addition of electrons from ionized acceptor atoms by residing closely to the *valence* band on the p-

side. Figure 3.4 depicts the subsequent unbiased p-n junction energy diagram. [Ref. 8, p. 83-87][Ref. 10, p. 70-78]

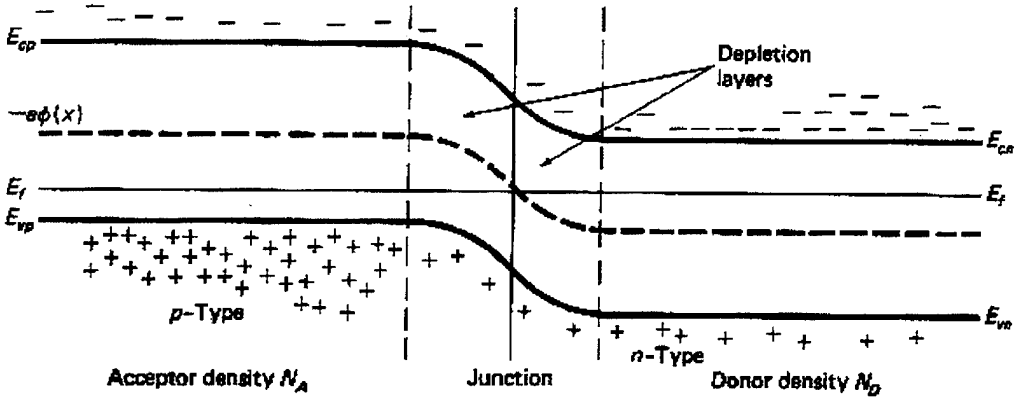

Figure 3. 4 Unbiased p-n junction potential energies. From [Ref. 8, p. 86]

The width, W, associated with this abrupt junction depletion region is found using

$$W = \sqrt{\frac{2\varepsilon_s}{q}\left(\frac{N_A + N_D}{N_A N_D}\right)\phi_o} \qquad \textbf{(3. 13)}$$

where

ε_s = Permittivity of Silicon (F/cm)
q = Charge of an electron (Coulomb)

2. The Biased Depletion Region

If an external force or biasing voltage were applied to the p-n junction, the total electrostatic potential will change and a change in the depletion width will follow suit. For example, if a positive voltage, V_o, were applied as in Figure 3.5, to the p-side with respect to the n-side, the p-n junction becomes forward biased. The electrostatic potential becomes ϕ_O - V_o and the potential barrier height reduces to q(ϕ_O - V_o). Conversely, by reversing the polarity to (-V_o), the electrostatic potential becomes ϕ_O - (-V_o), which is an increase and a consequent increase in the barrier height. This is called reverse biasing.

The corresponding Fermi level no longer remains constant but is now the difference between the two Fermi levels on either side of the junction. In other words, E_{fpo}-E_{fno} = qV_O. This phenomenon be seen in Figure 3.6. This potential barrier height corresponds to inhibiting majority carriers from crossing the junction. However, as in Figure 3.6, it induces minority carriers to cross the junction, hence becoming majority carriers. "In essence, the presence of an external voltage across the junction strongly affects the minority carriers, but affects the majority carriers very little." [Ref. 8, p. 89]

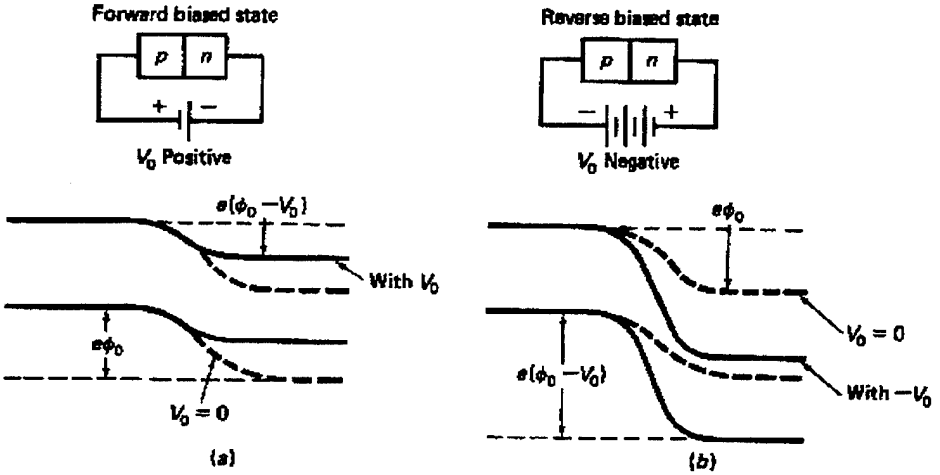

Figure 3. 5 Biased p-n junction potential energies. From [Ref. 8, p. 88]

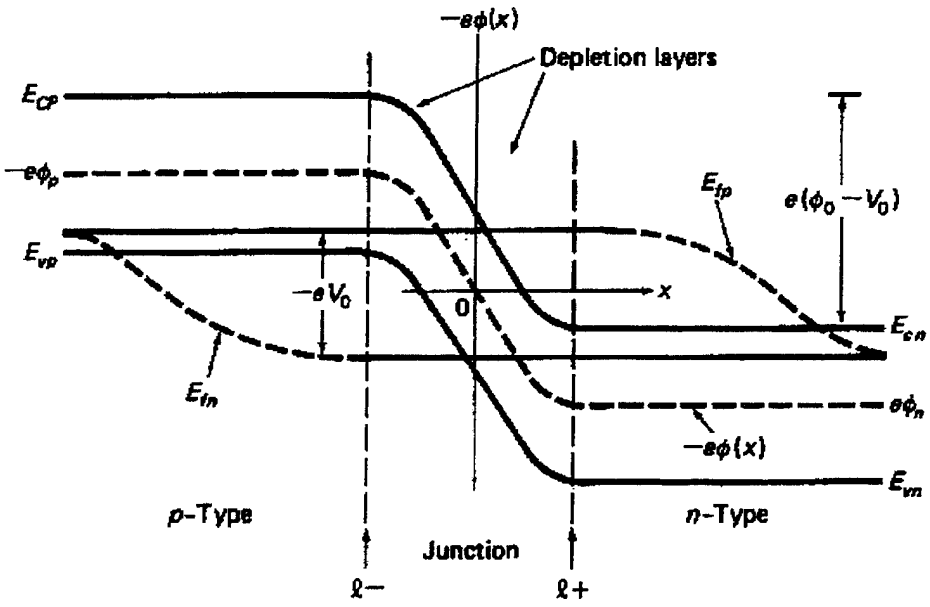

Figure 3. 6 Energy band potentials and Fermi levels with an applied external voltage. From [Ref. 8, p. 89]

The corresponding biased depletion width is found by modifying Equation 3.13 by adding a term for the bias voltage.

$$W = \sqrt{\frac{2\varepsilon_s}{q}\left(\frac{N_A + N_D}{N_A N_D}\right)(\phi_o - V_o)} \qquad \textbf{(3. 14)}$$

Thus, a positive bias voltage will decrease the depletion width while a reverse bias will extend the width. [Ref. 10, p. 80]

IV. MOS CAPACITOR FUNDAMENTALS

There are two types of semiconductor capacitors normally used to internally compensate an operational amplifier: junction and MOS (also called oxide) capacitors. Since spacecraft power usage is of the most critical concern and MOS type circuits offer much lower power consumption, the scope of this research was narrowed to include only the MOS type capacitor. Before any examination of radiation effects can take place there must be some understanding as to the construction and fundamental operation of this type capacitor.

A. THE CAPACITOR STRUCTURE

Metal Oxide Semiconductor (MOS) or 'oxide' capacitors, also known as MOS diodes, are created by growing a thin layer of SiO_2 (the oxide), which behaves as the dielectric material, between two conducting plates. Figure 4.1 shows a typical layout and cross section view. Normally, a thin sheet of aluminum deposited over the oxide forms the top plate while a region of low resistivity silicon supporting the oxide layer is used for the bottom. [Ref. 11, p.164]

1. Bottom Plate Formation

As seen in Figure 4.1, the lower plate of the capacitor is formed by placing an n+ emitter diffusion layer of silicon inside an n-type well which is formed on top of a p-type substrate.

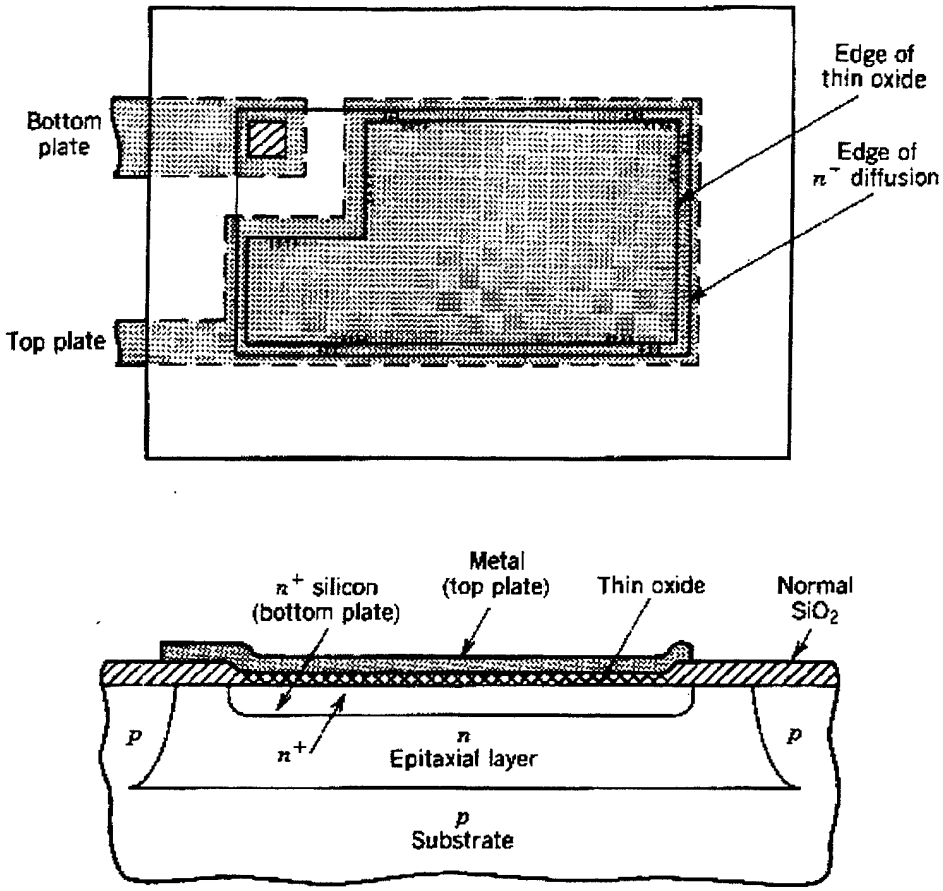

Figure 4. 1 Layout and cross sectional view of a typical MOS capacitor. [Ref. 11, p. 164]

a. Sheet Resistance and Lower Plate Parasitics

Inherent to the capacitor is a parameter called the sheet resistance, R_S. The resistance of a material having dimensions length L, width W and thickness T is given by

$$R = \frac{\rho L}{TW} \qquad \textbf{(4. 1)}$$

where

ρ = material resistivity (Ω/cm)

Integrated circuit manufacturers prefer to use a similar parameter called the sheet resistance. It is defined as

$$R_s = \frac{\rho}{T} \qquad \textbf{(4. 2)}$$

The sheet resistance has units of ohms per unit square. To find the total resistance of a given size material, simply multiply the sheet resistance by the length to width ratio. Ideally, the resistance of the capacitor dielectric material is zero. Since this, however, is not physically possible, sheet resistances of a few ohms are typical.

Other device parasitics include a stray capacitance of the substrate and epitaxial layer p-n junction and the accompanying reverse-biased collector substrate diode. The entire MOS capacitor equivalent circuit is illustrated in Figure 4.2. It is common during the manufacturing process to minimize the parasitic capacitance by decreasing or completely eliminating the n-type epitaxial layer. [Ref. 11, p. 164-166]

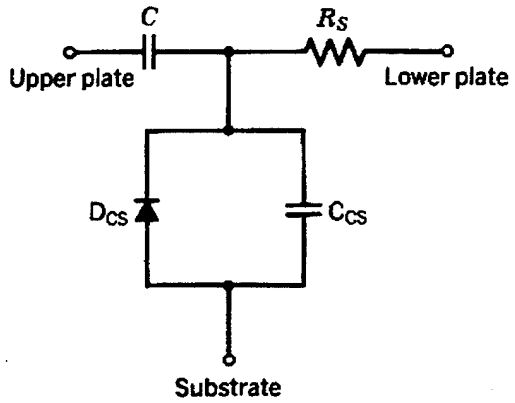

Figure 4. 2 MOS capacitor electrical equivalent circuit diagram. [Ref. 11, p. 165]

b. Emitter Diffusion

One possible way to construct the bottom plate is by using n+ emitter diffusion. Diffusion is the mechanism whereby differing types of particles occupying a given volume tend to spread out and redistribute themselves evenly throughout this volume. Particle diffusion may occur via two mechanisms: substitutional or interstitial. In substitutional diffusion the impurity atoms replace a silicon atom at a lattice site. Interstitial diffusion involves the impurity atoms occupying an interstitial void. Integrated circuit manufacturing is primarily concerned with the first type of diffusion. These particles diffuse according to Fick's Law. This law states that the net particle flux density, F, varies by

$$F = -D\frac{\partial N}{\partial x} \qquad \textbf{(4. 3)}$$

where

N = # particles/unit volume
x = distance measured parallel to flow direction
D = diffusion coefficient (length^2/time)

The negative sign indicates the diffusion direction from regions of higher to lower concentration. The diffusion coefficient provides a measure of movement difficulty the impurity particles feel in the lattice structure. It is a property of the impurity and varies exponentially with temperature. Thus in n+ diffusion, a controlled, large amount of dopant is introduced into n-type silicon, allowed to diffuse and become the bottom plate of the MOS capacitor. [Ref. 11, p. 6-7]

2. Oxidized Dielectric Layer

The thin oxidized layer of silicon, which forms the dielectric region, is generated by heating the silicon wafer to a temperature range of 900-1200°C. An inert carrier gas which contains the oxidizing agent is passed over the wafer surface and according to the chemical reaction

$$Si + 2H_2O \rightarrow SiO_2 + 2H_2 \qquad \textbf{(4. 4)}$$

The presence of water vapor on the left hand side acts to significantly expedite the oxidation process. The oxidation proceeds inward from the surface and slows as the oxidation thickens. For thin layers, a linear growth rate is achievable with respect to time. As the layer thickens, however, the growth rate becomes proportional to the square root of time. Practical thickness of thermally grown SiO_2 used for integrated circuits are in the range of 0.05-2 μm. The lower limit is set by electrical breakdown voltages, process control or random defect densities (i.e., pin holes) in the oxide layer whereas the upper limit is determined by acceptable oxidation times and difficulty of oxide etching during the photo-masking step. [Ref. 11, p. 16]

3. Top Plate Construction

The final step in preparing the MOS capacitor is to deposit an extremely thin layer of conductive material, usually aluminum, on top of the oxide layer. As viewed in Figure 4.1, this top plate completely covers the dielectric and bottom plate. The metal can be deposited by a variety of methods, two of which will be briefly discussed here.

a. Vacuum Evaporation

The capacitor is placed with the conductive element to be evaporated in a bell jar vacuum chamber where pressures range from 10^{-5} to 10^{-6} torr. The metal is heated until vaporization occurs. "Under the high-vacuum conditions used, the mean free path of the vaporized molecules is comparable to the dimensions of the bell jar. Therefore the vaporized material radiates in all directions within the bell jar." [Ref. 11, p. 23] The oxide layer is placed to receive a nearly uniform covering of this vaporized metal and is kept at higher temperatures to ensure good adhesion.

b. Cathode Sputtering

Also in a low pressure environment, but this time occurring with a gas medium, a sputtering apparatus is constructed. A potential of approximately 5000 V is applied between a cathode coated with the conductive element and an anode with the oxide layer attached forming a glow discharge. The gas commonly used is argon (A). Positively ionized argon atoms generated by this glow discharge accelerate toward the negatively charged cathode. They then impact the cathode and knock off (sputter) metal atoms some of which deposit themselves on the oxide layer. Cathode sputtering is much slower than vacuum evaporation.

B. FUNDAMENTAL MOS CAPACITOR OPERATIONS

MOS capacitors, unlike their junction counterparts, can operate with either positive or negative bias applied across the plates. [Ref. 11, p. 165] This section first examines the ideal capacitor response to differing bias conditions. Then a discussion on non-ideal work function differences, interface traps and oxide charges is offered.

1. The Ideal Capacitor

When there is no applied voltage to the previously studied p-type substrate capacitor, the work function difference, $q\phi_{ms}$, is ideally zero. This work function difference, in Equation 4.5 and graphically depicted in Figure 4.3, is defined by the energy difference between the metal work function, $q\phi_m$, and the semiconductor work function, $q\phi_S$.

$$q\phi_{ms} \equiv q\phi_m - (q\chi + \frac{E_g}{2} + q\psi_B) = q\phi_m - q\phi_s = 0 \qquad \textbf{(4. 5)}$$

where

$q\chi$ = semiconductor electron affinity

$q\psi_B$ = energy difference between the Fermi and intrinsic Fermi levels

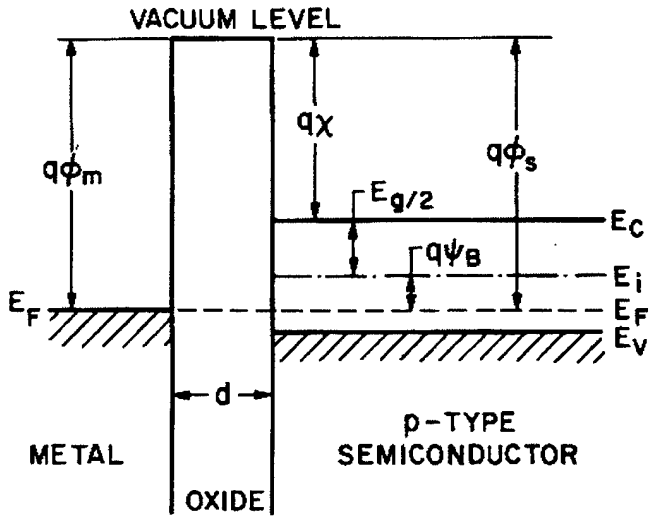

Figure 4. 3 Flat band energy diagram. From [Ref. 10, p. 187]

The conduction and valence bands under a no bias voltage condition appear flat. This voltage is called the ideal flat band voltage. There are two other defining characteristics for the MOS capacitor. First, there is no carrier transport through the oxide layer. In

other words, the resistivity of the oxide is considered infinite. Second, the only existing charges regardless of the biasing conditions are those existing in the bottom plate surface and those on the top metal plate adjacent to the oxide layer. [Ref. 10, p. 187]

a. Accumulation

As different biasing voltages are applied to the capacitor, three possible cases may exist at the semiconductor surface. If a negative voltage, where the polarity is from the top plate with respect to the bottom, mobile holes are attracted to the surface and the energy bands near the p-type semiconductor surface are bent upward. No current will flow in an ideal case regardless of the polarity or magnitude of the voltage applied. This keeps the Fermi level constant. Recall that the semiconductor carrier density varies exponentially with the energy difference between E_f, Fermi level and E_i, one half of the band gap energy.

$$p = n_i \exp[(E_i - E_F) / kT] \qquad \textbf{(4. 6)}$$

It can be easily seen in Figure 4.4a how the energy difference term increases as the bands bend up. This causes an increase, or accumulation, in the number of holes near the oxide-semiconductor boundary.

b. Depletion

If a small positive voltage were applied to the capacitor, the energy bands bend down and the energy difference decreases. The majority carrier holes are then depleted in a region possessing a width, W, as seen in Figure 4.4b.

c. Inversion

Finally, if the voltage is increased, the energy bands continue to bend downward until the intrinsic level crosses the Fermi level. (See Figure 4.4c) Similarly to Equation 4.6, the electron concentration varies as

$$n = n_i \exp[(E_F - E_i) / kT] \qquad \textbf{(4. 7)}$$

Since the Fermi level is now higher than the intrinsic level, (E_f-E_i) will be positive and the concentration of electrons will increase. The number of minority carrier electrons will exceed the number of majority carrier holes and the resulting surface is called inverted. If the voltage is further increased, the conduction band will approach the Fermi level which causes the electron concentration to rapidly expand. Any further voltage increase will ensure a collection of a very thin layer of additional negative charge called the inversion layer. Typically, the width of this layer is much smaller than the width of the surface depletion layer. Once this inversion layer has formed, the surface depletion layer width, W, reaches a maximum found by

$$W_{\max} = \sqrt{\frac{4\varepsilon_s kT \ln(N_A / n_i)}{q^2 N_A}} \qquad \textbf{(4. 8)}$$

Once the bands are bent to induce this strong inversion, any further bending will result in a very small increase in the depletion layer width but a corresponding large increase in the total charge in the newly formed inversion layer. [Ref. 12, p. 3-16] [Ref. 10, p. 186-189]

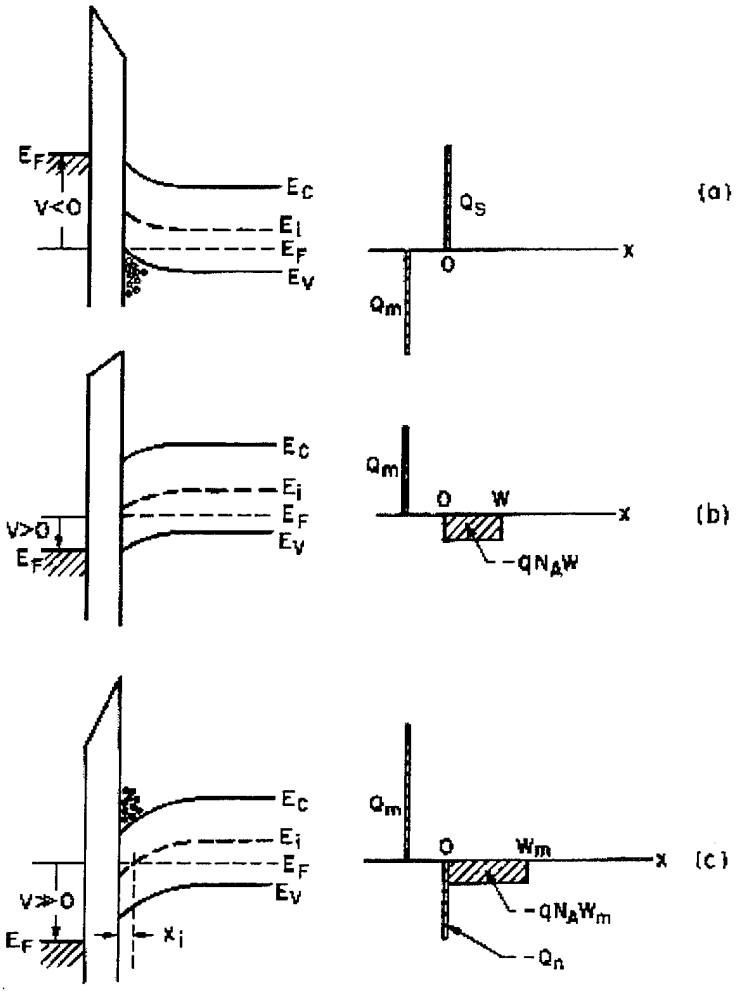

Figure 4. 4 Ideal MOS capacitor Energy band diagrams and charge distributions. (a) Accumulation. (b) Depletion. (c) Inversion. From [Ref. 10, p. 188]

d. Ideal Capacitance Calculation

The total ideal MOS capacitance consists simply of the series connection of the capacitance of the oxide layer between the metal plate and the substrate, C_{ox}, and the depletion layer capacitance, C_S. In other words, the total capacitance satisfies $C^{-1} = C_{ox}^{-1} + C_s^{-1}$. Recall $C_S=\varepsilon_S/W$, that is, the depletion layer capacitance per unit area is the bulk silicon permittivity divided by the depletion width, given in Equation 3.14. Then the total to oxide capacitance ratio may be found by Equation 4.9

$$\frac{C}{C_{ox}} = \frac{1}{\sqrt{1 + (2\varepsilon_{ox} V_g / qN_A \varepsilon_s t_{ox}^2)}} \qquad \textbf{(4. 9)}$$

where

V_g = Gate voltage
ε_s = silicon permittivity
ε_{ox} = oxide permittivity
t_{ox} = oxide thickness

2. Non-Ideal Considerations

a. Work Function Difference

When examined ideally, the work function difference, q_{ms}, was determined to be zero. In reality, it is not zero and normally $q\psi_m$ is smaller than $q\psi_s$, which means ($q\psi_m$ - $q\psi_s$) is negative. Thus, some electrons are able to leave the metal and reach the p-type silicon via an external path which is more conductive than the highly resistive oxide layer. The metal gate becomes slightly positively charged and repels holes while uncompensated negative acceptors appear near the semiconductor surface. This charge separation forms a potential difference shared by both the oxide and the depletion region and is equal in magnitude but opposite in sign to the work function q_{ms}. [Ref. 10, p. 195-197] [Ref. 12, p. 3-6]

b. Trapped, Fixed and Mobile Oxide Charge

In addition to the work function difference, interface trapped, oxide trapped, fixed oxide, and mobile ionic charges exist within the capacitor. [Ref. 13, p. 606] Interface trapped charges, Q_{it}, are due to attributes at the Si-SiO_2 interface and are largely dependent on the chemical structure at this interface during production. The traps are located in the interface with energy states in the forbidden gap for silicon. The

density of interface traps is dependent on the orientation of the crystal structure described by Miller indices and illustrated in Figure 4.5. It is believed that interface trap densities increase with respect to the order <100>, <110>, <111>, with an order of magnitude difference between the two extremes and a value of Q_{it} *<111>* equal to one charge per 10^4 surface atoms. To reduce Q_{it} during production, MOS capacitors with thermally grown silicon dioxide on silicon are thermally annealed at low temperature (450°C). Interface traps, as discussed in Chapter V, may also be generated by ionizing radiation sources. [Ref. 10, p. 197] [Ref. 12, p. 6-19] [Ref. 14, p. 573]

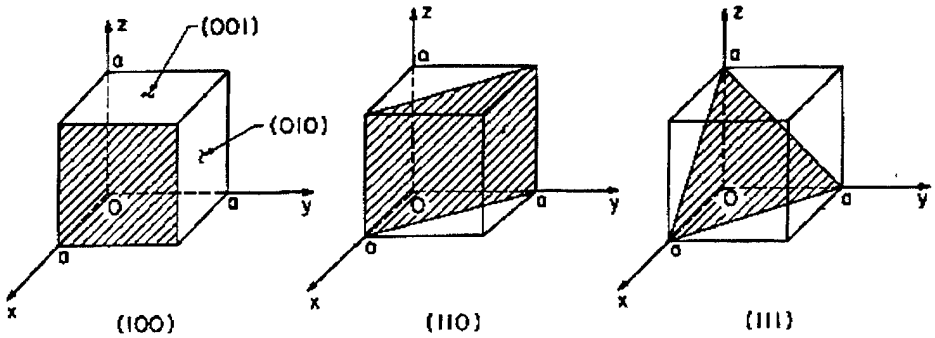

Figure 4. 5 Illustration of three Miller indices. From [Ref. 10, p. 7]

The next type of non-ideal charge is called the fixed oxide charge, Q_f. This charge is located within 30 Angstroms of the Si-SiO_2 interface and as the name suggests, it is fixed, normally positive and is dependent also on orientation as well as oxidation and annealing conditions during production. A possible explanation for their existence is that shortly after the growth of the oxide layer, there is thought to be ionic silicon and uncompleted silicon bonds remaining at near surface. Fixed oxide density for a <111> orientation is about $5x10^{10}$ per cm^2 and are five times greater than <100>. The <100>

orientation is preferred in MOS capacitor production due to the combined lower values of charges for Q_f and Q_{it}. [Ref. 10, p. 198]

The third charge types are the mobile ion charges, Q_m, such as sodium or other alkali metals. These ions are largely the result of contamination during capacitor construction. Since they are highly mobile, especially at higher temperatures, and positive, they will be pushed toward the Si-SiO_2 interface with an applied positive gate voltage. This results in a large change in system capacitance. However, this change is not permanent as it is with the fixed charge. The capacitance will shift back again with the application of a negative bias as the ions become attracted to the negative plate. The relative ease in redistributing the mobile charges is a cause for device instability. In order to reduce these contaminants, precautions such as furnace wall cleaning (often with hydrochloric acid gas or chlorine), gas purification during the oxidation process and ensuring the silicon crystal surface and chemicals used in fabrication are all as pure as possible. [Ref. 12, p. 21]

The final non-ideal charges are called oxide trapped charges, Q_{ot}. These are charges trapped inside the silicon dioxide layer. They may be created by exposure to radiation sources such as X-rays or high energy electrons as discussed in Chapter V. A summary of interface traps and oxide charges is offered in Figure 4.6.

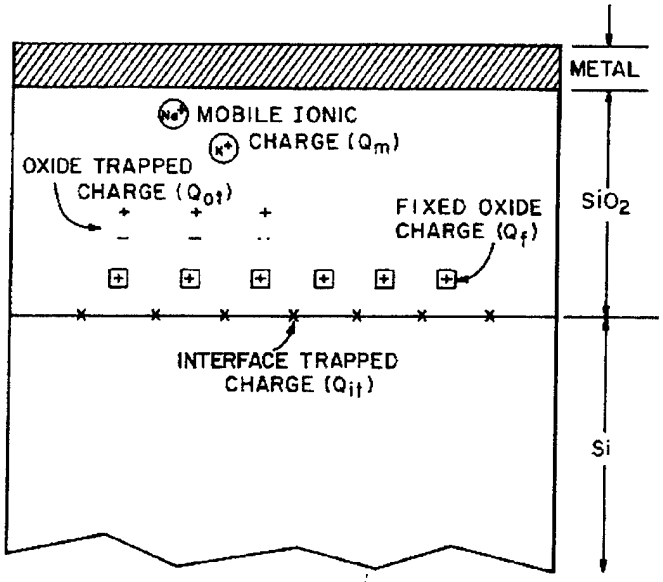

Figure 4. 6 Depiction of non-ideal charges and traps. From [Ref. 10, p. 197]

c. Flat Band Voltage

The sum effect of all the aforementioned non-ideal charges is to change the value of the ideal flat band voltage. The governing equation for V_{FB} becomes

$$V_{FB} = \phi_{ms} - \frac{Q_f + Q_m + Q_{ot}}{C_o} \qquad \textbf{(4. 10)}$$

In other words, the flat band voltage is shifted by an amount in the last term in Equation 4.10. Figure 4.7a shows the ideal C-V curve for the MOS capacitor and Figure 4.7b depicts the shift due to a non zero work function difference and all oxide charges. Finally, if there are large amounts of interface trapped charges, Q_{it}, the C-V curve will be not only displaced but the shape will also vary. This is shown in Figure 4.7c.

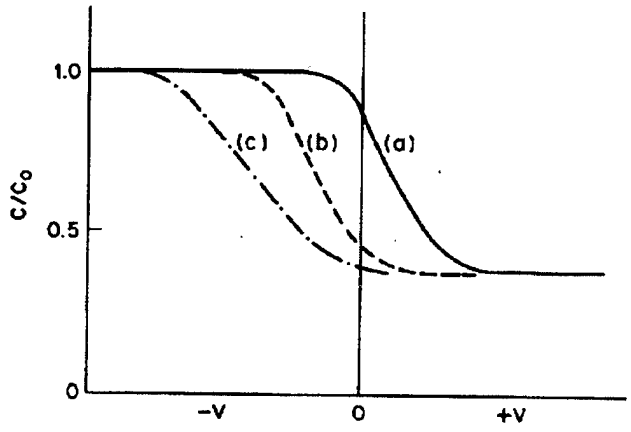

Figure 4. 7 C-V curve shift with oxide charges and interface traps. [Ref. 10, p. 200]

C. CMOS VS. MOS TECHNOLOGY

CMOS or Complimentary Metal Oxide Semiconductor technology offers many benefits when compared to MOS such as high speed operation, low power dissipation and fewer defect densities during manufacturing, just to name a few. Construction consists of a pair of transistors on the same substrate, typically p-type. One transistor is fabricated directly on top of the substrate (n-channel enhancement mode) while the other rests in a 'well' of n-type substrate (p-channel enhancement mode). A CMOS or MOS transistor may emulate a capacitor by biasing the gate and leaving the source and drain connections floating.

V. RADIATION DAMAGE MECHANISMS

The natural space radiation environment contains many particles that may disturb the normal function of electronic circuits. Chapter II discussed particle types present and their corresponding locations in the natural space environment. "The manner in which radiation interacts with solid material depends on the type, kinetic energy, mass, and charge state of the incoming particle and the mass, atomic number and density of the target material." [Ref. 5, p. II-14] Attention is now turned to the physical interactions between these particles and silicon and silicon dioxide. Radiation effects can be grouped into two broad classes: (1) ionizing radiation effects due to electron-hole pair production and (2) displacement effects due to high energy particles.

A. IONIZATION

1. Charged Particle Effects

Ionization is the creation of electron-hole pairs resulting from charged particle collisions with electrons bound to atoms in the target material lattice. These collisions must provide enough energy to elevate electrons into the conduction band corresponding to additional valence band holes, causing an electron-hole pair. Ionization effects are not a function of the type of particle. Rather, the governing parameter is the energy loss of the particle during collision. Consequently, the number of pairs produced is proportional to this loss. The minimum energy needed to create and electron-hole pair, *Ep*, in silicon and silicon dioxide is 3.6 and 17eV respectively. As long as the colliding particle energy is greater than *Ep*, electron-hole pairs will continue to be created. For this reason, a

single high energy proton or electron can be responsible for creating thousands or millions of pairs. Due to their abundance in the magnetosphere, high energy electrons and protons produce the vast majority of ionization damage to Earth-orbiting satellites, although heavy ions and photons also are capable of ionizing MOS capacitor material. [Ref. 5, p. II-17] [Ref. 14, p. 550]

2. Photon Effects

Photons are not a primary concern for ionizing damage in the natural space environment. However, a short discussion is required since emission of either low energy x-rays or high energy gamma rays are common to most laboratory sources used to simulate space radiation effects. There are three primary interactions of emitted photons with material, all terminating with the creation of energetic electrons.

a. Photoelectric Effect

Photons with energies below 70 keV interact predominately through the photoelectric effect. The target atom absorbs an incident photon which excites an electron from either an inner shell or the valence shell of the target atom to a threshold energy level allowing liberation from the atom. This creates an electron and a positive ion; the electron-hole pair. For the inner shell case, an outer shell electron from the same atom then drops into the lower shell, emits a photon which can, depending on energy level, repeat the ionization process.

b. Compton Effect

For photons with energies between 70 keV and 20 MeV, the dominant mechanism is called Compton scattering. During this process, the incident photon is not

completely absorbed but transfers a sufficient fraction of its energy to an electron in the target atom allowing it to be released. Thus, a electron-hole pair is created along with a lower energy 'Compton' photon, which again is free to interact in the lattice.

c. Pair Production

Providing the incident photon has in excess of 1.02 MeV, pair production is possible. Upon collision, the photon is completely annihilated and an electron-positron pair is produced. A positron has the mass of an electron but an opposite charge. Energy in excess of 1.02 MeV is evenly distributed between the electron and positron as kinetic energy. It should be noted that photons with energy great enough to produce electron-positron pairs are not normally encountered in the natural space environment. The three photon mechanisms as functions of energy and target atomic mass are illustrated in Figure 5.1. [Ref. 14, p. 552]

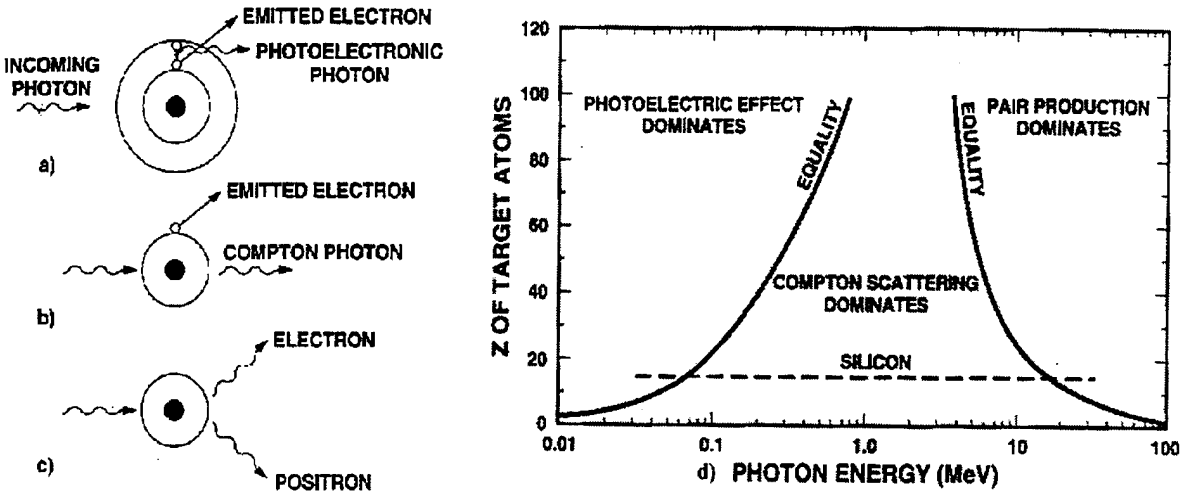

Figure 5. 1 Photon interaction (a) for photoelectric, (b) Compton, (c) pair production, (d) as functions of energy and atomic mass. After [Ref. 5, p. II-15-16]

3. Dose Enhancement

Another mechanism which determines the total number of electron-hole pairs created is called dose enhancement. This only occurs when the incident particle travels through two adjacent materials with differing atomic masses, as in silicon and silicon dioxide. At the interface, charge particle equilibrium, defined as the total energy carried into a mass element by electrons equals the total energy carried out by electrons, is not maintained. The relative dose ratio in the two materials may be expressed as

$$\frac{D_{eq}(1)}{D_{eq}(2)} = \frac{(\mu_{en}/\rho)_1}{(\mu_{en}/\rho)_2} \qquad \textbf{(5. 1)}$$

where

$D_{eq}(1,2)$ = relative dose ratio of materials 1,2
μ_{en} = mass energy absorption coefficients
ρ = material densities

The dose received at the interface is not only direction dependent but is also a function of the mechanism employed by the incident photon, i.e., photoelectric, Compton, etc. It will be largest for low energy photons (<< 1MeV) interacting through the photoelectric effect. [Ref. 15, p. 4369]

B. DISPLACEMENT/DEFECT CENTERS

Energetic particles and photons can also be responsible for another damage phenomenon called displacement damage. As the name implies, incident particles colliding with an atom while possessing a minimum displacement threshold energy can force the atom to recoil from its lattice site and create an interstitial. Displacement damage is rare when compared to the ionization events discussed above, however,

displacement damage can create permanent damage to the lattice structure. Whereas ionization depended solely on the energy of the particle and not particle type, displacement damage is highly dependent on particle type. For example, energetic protons are much more adept at producing displacements than are electrons. [Ref. 14, p. 553]

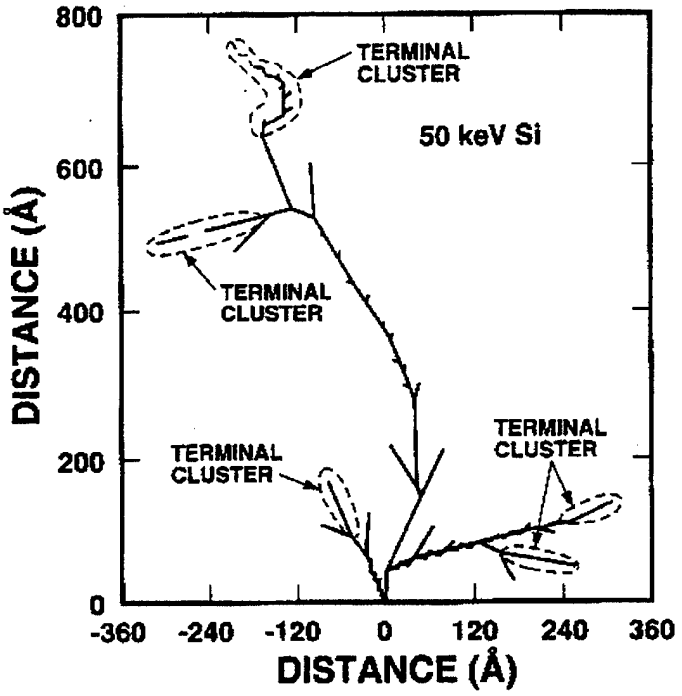

Figure 5. 2 Defect Cascade demonstration. After [Ref. 17]

In addition to the displacement damage, quite a considerable amount of ionization is possible as many valence bonds are broken when the atoms displace. The interstitial/vacancy pair is referred to as a close or Frenkel pair and an incident particle must have at least 21 eV to create a Frenkel pair in silicon. [Ref. 16, p. 228-239] There are various types of defects which can occur in irradiated silicon. A simple or point defect contains one defect site, whereas higher energy particles can create a cascade of

defects resulting in defect clusters. Figure 5.2 shows a defect cascade and associated terminal clusters resulting from a 50 keV recoil atom.

1. Defect Center Electrical Effects

Radiation induced defects have associated energy levels which reside between the conduction and valence band. These defect energy states impact the electrical behavior of semiconductor devices. The basic device defect degradation process is as follows:

1. Incident particles displace atoms
2. New energy levels are created by the defects
3. These new levels alter device electrical properties

Associated with the above list are five possible electrical effects which can occur. The first is called thermal generation of electron hole pairs and is possible when the defect energy level is midway between the conduction and valence band. A valence band electron is bound at the defect center and is thermally excited to the conduction band, generating an electron-hole pair. The generation of pairs tapers off exponentially as the defect energy moves away from midgap toward the conduction band. The second effect, recombination, is a process where a carrier of either sign is captured by a defect center followed by a carrier of the opposite sign, resulting in a removal of the electron-hole pair. The third effect is a trapping of carriers at shallow levels in the energy band. That is, an electron can be trapped near the conduction band while a hole can be trapped near the valence band. The capture can be temporary with the carrier later emitted into its respective band without recombining. The next effect is labeled compensation. Here, some of the available electrons are compensated by 'deep-lying' radiation induced holes. Equilibrium majority carrier concentration is therefore reduced. The last process is called

carrier tunneling. The trap assists carriers across the bandgap which results in increased current in the device. All five effects are depicted in Figure 5.3. [Ref. 18, p. 1446-1447][Ref. 5, p. II-20]

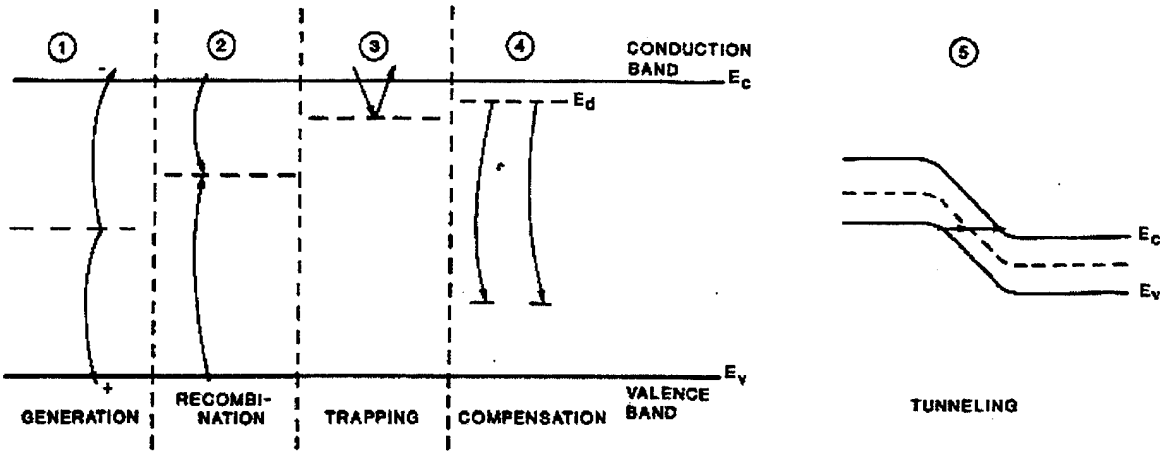

Figure 5. 3 Defect center electrical effects. After [Ref. 18, p. 1446]

C. TRAPPED CHARGES

Ionization and defect centers collaborate to form charge trapping centers in both bulk silicon and silicon dioxide. Charge trapping literally means to hold a charge at a trapping site within the material. Possible options are oxide traps, interface traps and a relatively new classification called border traps. They are considered below.

1. Oxide Traps

Assume a positive bias is applied to the gate of the MOS capacitor. Immediately following ionizing radiation exposure and electron-hole creation in the oxide, some fraction of pairs will recombine before leaving the oxide. The remaining fraction that do not recombine constitute the electron-hole yield and determine the amount of charge which may be trapped. The yield is highly dependent on applied bias. With no bias, the

yield can approach zero pairs while a high bias can virtually eliminate any recombination. Recall electrons are much more mobile than the holes. They will swiftly migrate toward the gate (in nanoseconds [Ref. 18, p. 1451]) and holes will move toward the Si-SiO_2 interface (numerous orders of magnitude slower than the electrons) via hopping through localized states in the dioxide bulk. Approaching the interface, some fraction of the holes become trapped at defect sites, forming a positive oxide-trap charge or space charge in the oxide, previously alluded to in Chapter IV and shown in Figure 5.4.

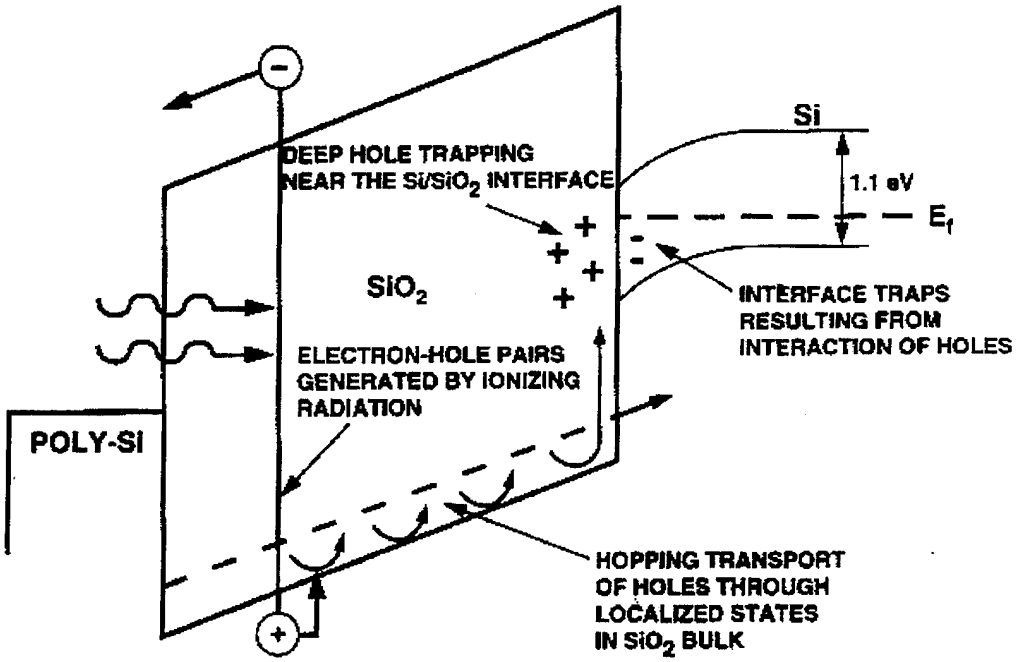

Figure 5. 4 Oxide and interface trap processes. After [Ref. 18, p. 1451]

2. Interface Traps

A defect which lies directly on the border of the Si/SiO_2 is named an interface trap. Interface traps have energy states within the silicon bandgap and are formed on two time scales under positive bias. The minority of interface traps are formed within

milliseconds of irradiation, while the vast majority are formed over thousands of seconds. Interface traps can communicate electrically with the silicon layer depending on the position of the trap energy level (E_t) with respect to the Fermi level, E_f. This relative energy difference allows interface traps to be either positive, negative or neutral. When $E_f < E_t$, the trap donates an electron to the silicon and becomes positively charged. Conversely, when $E_f > E_t$, the trap accepts an electron from the silicon and becomes negatively charged. When $E_f \approx E_t$, that is at midgap, interface traps have neutral charge. Interface trap charges do not anneal at room temperature and are very important to low dose rate applications, such as space. [Ref. 5, p. II-43] In earlier models, interface traps were thought to communicate electrically with the silicon layer while oxide traps were thought to be excluded from this process. As discussed below, present rationale has been modified.

3. Border Traps

It is currently acknowledged that it is not always possible to tell whether charge exchange with the silicon is due to a defect at the interface or within the oxide layer. A border trap classification has been created to explain the fact that near interface oxide traps, once thought to be fixed, can in fact exchange (switch) charge with the supporting silicon just as an interface trap discussed above. Figure 5.5 illustrates oxide, interface and border traps as well as the locations for switching and fixed states. [Ref. 19, p. 5058-5061]

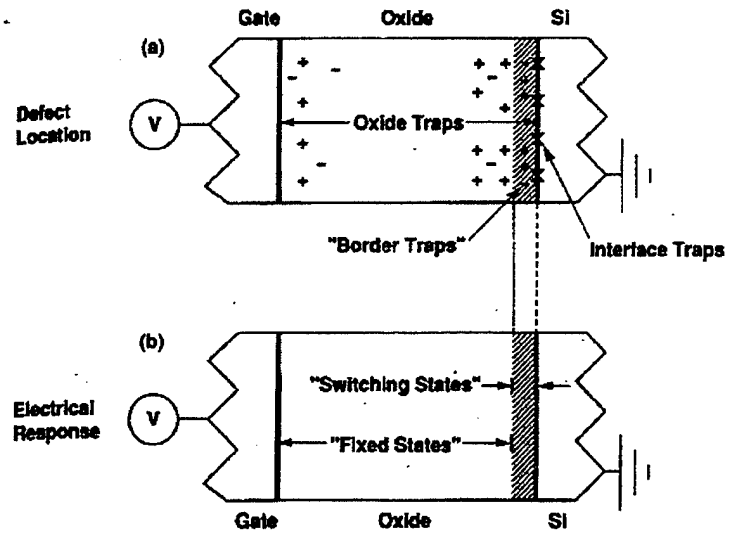

Figure 5. 5 Diagram of (a) physical location of defects and (b) their electrical response. From [Ref. 19, p. 5059]

D. SUMMARY

The principal ionization-induced charges in bulk material are conductivity increases through production of excess charged carriers (electron-hole pairs), trapped charges mainly in insulators, production of electric and magnetic fields and chemical effects. [Ref. 8, p. 277] Examining the oxide layer more specifically, ionizing radiation sources generate excess carriers which become trapped either in the oxide layer or at the interface. Irradiation can increase the conductivity of the insulator, but normally not enough to increase carrier recombination. Thus, recombination may occur for days after irradiation. This explains how charges may stay trapped at the defect centers leading to permanent degradation of the oxide layer while under continuous radiation effects in space.

VI. EXPERIMENTAL FORMATION

The primary aim of this research is to determine radiation damage effects on MOS capacitors used to internally compensate operational amplifiers on the same Very Large Scale Integrated (VLSI) circuit. Operational amplifiers are basic building blocks to all types of electronic circuits (including those aboard any spacecraft), such as filters and analog-to-digital converters. As will be shown, the 3dB (break) frequency and consequently, the frequency bandwidth of a filter passed is determined partially by this capacitor. The need for stable, predictable performance and graceful aging throughout the filter lifetime, thus ensuring passing of the designed spectra, is an essential element toward accomplishing the spacecraft mission. The need to separate the capacitor from the remaining elements of the amplifier circuit is a crucial step toward determining the contribution of amplifier degradation or enhancement due uniquely to the irradiated capacitor.

Previous research has measured radiation damage effects of MOS capacitors by analyzing high frequency and/or low frequency quasi static capacitance-voltage (C-V) curves. [Ref. 5, p. II-22] Winokour, et. al., irradiated a positively biased MOS capacitor composed of a p-type substrate, 50.3nm thick oxide with a corresponding capacitance of 78.5pF. The capacitor received a total of 1 Mrad(SiO_2) with a dose rate of ≈240 rad (SiO_2) per second. [Ref. 20, p. 1454] It can readily be seen in Figure 6.1 how the capacitance decreased with increasing dose received.

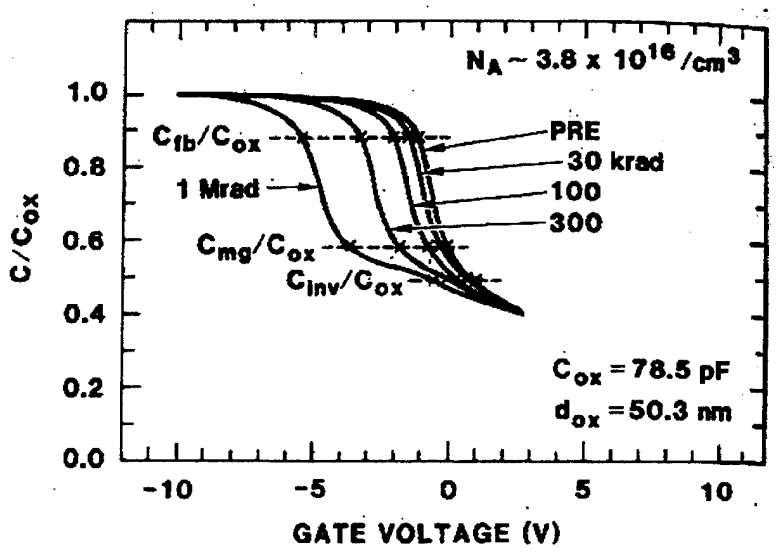

Figure 6. 1 C-V curve shift with increasing radiation dose. From [Ref. 20, p. 1454]

According to simple operational amplifier theory [Ref. 21, p. 3.9], it is known that if the compensating capacitor value changes, the corresponding closed loop 3 dB break point or roll-off point will change according to

$$f_{3dB} = \frac{1}{2\pi R_o C_c} \qquad \textbf{(6. 1)}$$

where

$f3dB$ = Break frequency (Hz)
R_O = Resistor value (Ohms). See Figure 6.3
C_C = Compensating capacitor (Farads)

It is readily seen that with a decrease in capacitance, the corresponding 3dB frequency will increase, thus enhancing our filter. It seemed counterintuitive that a space-borne filter, irradiated by the space environment, would have *increased* capability as it aged in orbit.

A. SELECTION OF THE OPERATIONAL AMPLIFIER

A new approach to the problem was therefore attempted. Until this research, there has been no known attempt of in-situ measurement of filter performance while a capacitor is exposed to a radiation source. Antecedent research at the Naval Postgraduate School produced integrated circuit chips containing composite amplifiers with compensating capacitors. They are labeled ISI NA3B HG2 #1-#4. The chips were manufactured using the fully custom MOSIS process, which used two-micron technology. This meant the minimum transistor gate length could be two microns [Ref. 22, p. 23-24]. The selected chip was placed in a dual in line package (dip) with 40 pins. It had two sets of Modified Open-circuit Floating Resistor (MOFR) and Toggled Switched Capacitor (TSC) amplifiers for a total of four amplifiers. See Figure 6.2 for a complete diagram of the integrated circuit used in the experiment. The reader is invited to read [Ref. 22, p. 118] for a list of references pertaining to these types of composite amplifiers.

Each amplifier has a corresponding internally compensating capacitor suitable for irradiation and discussed below. It was decided to build a simple low pass filter from discrete parts. Since there were four capacitors per chip, four filters were constructed using the capacitors, two LM-747s (twin op-amps in a single package with 14 pins) and two resistors per amp chosen to provide suitable gain. A schematic, representative of each of the filters (drawn with the P-Spice CAD Tool) is depicted in Figure 6.3.

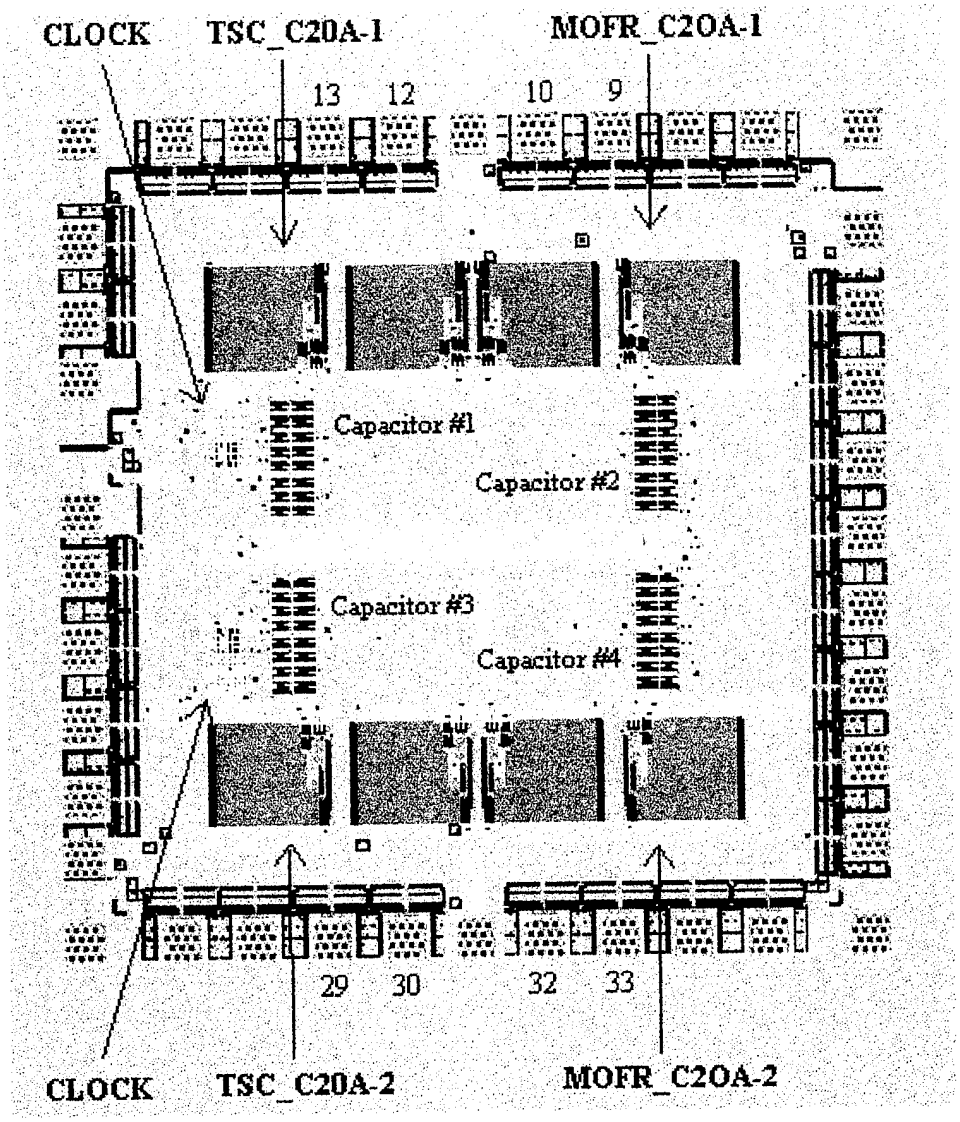

Figure 6. 2 MOSIS Integrated circuit layout. From [Ref. 22, p. 76]

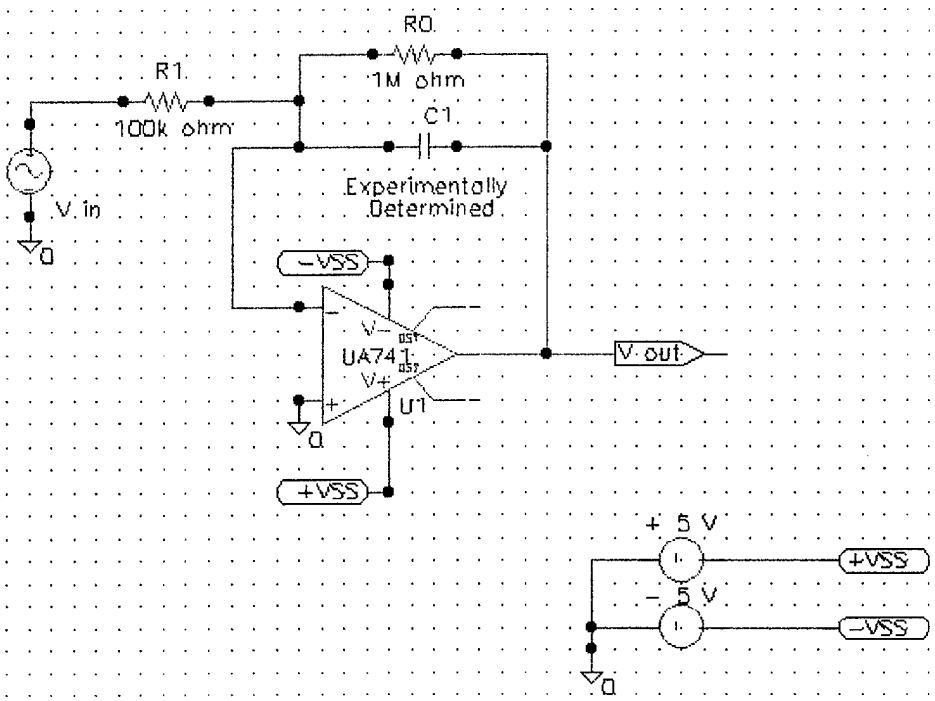

Figure 6. 3 Representative schematic of the low pass filter.

Since composite amplifiers were on the same chip as the capacitors, a unique opportunity arose to examine their radiation response along side the capacitors. After it was determined that the individual amplifiers comprising the composite were accessible, that is, the inputs and output could be obtained via pinouts, tests were conducted to validate their operation. Unfortunately, there seemed to be a malfunction with the two phase non-overlapping clock circuit, critical to the operation of a switched capacitor circuit, which rendered them inoperable prior to the experiment. Therefore, only one experiment could proceed.

B. THE COMPENSATING CAPACITOR

The selected capacitor used to compensate the operational amplifier was constructed of a top and bottom metal plate, separated by an oxide layer, residing on a field oxide on top of a substrate. This is shown in Figure 6.4. As seen in the diagram, the

total capacitance is the parallel plate capacitance, C_p, in parallel with two capacitances, C_m and C_b, which are metal plates to substrate parasitic capacitances. According to [Ref. 23, p. 43-68], "these parasitic capacitances do not degrade the performance of the circuit due to stray insensitive topologies used." [Ref. 22, p. 45]

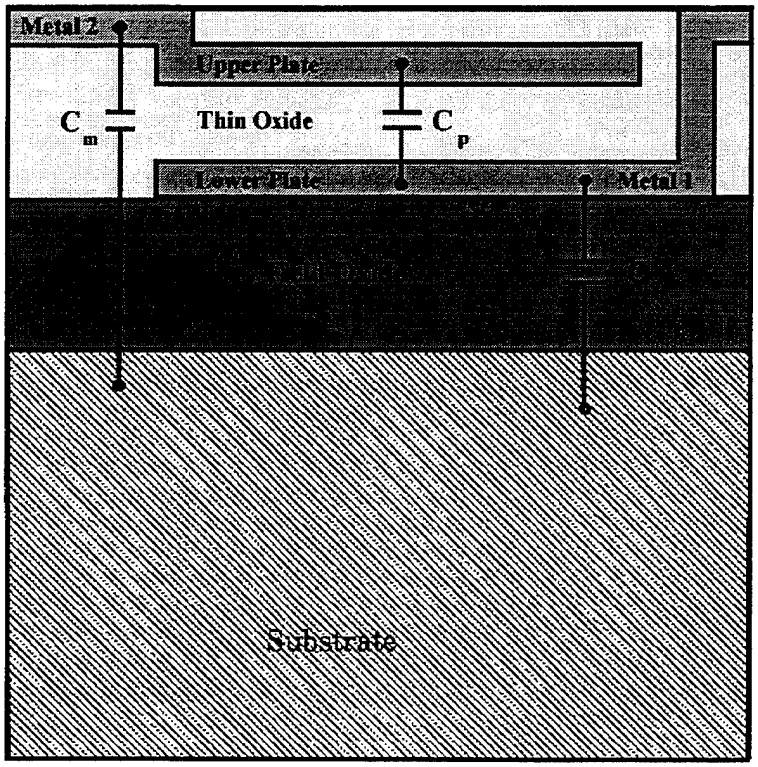

Figure 6. 4 Parallel plate capacitor cross section. After [Ref. 22, p. 46]

The research by Silvernagel was partly an exercise in reducing capacitor layout size while ensuring an accurate capacitor ratio for a specific switched capacitor design. Therefore, a design was chosen, depicted in Figure 6.5, which has a central capacitor surrounded by a ring of 5 exact replicas plus one scaled by a small factor. There is a slight enlargement of the lower right capacitor, giving a ring-to-center capacitance ratio of 6.11:1. [Ref. 22, p. 47] Target capacitance was 0.5-2.0 pF for each square. This would

give a range of capacitance for the filter application of 0.5-14.0 pF. The lower limit is of a single square minimum and the latter is upper limit of the center square and ring connected in parallel. Since these are extremely small capacitance values, the decision was made to maximize the total capacitance and connect the center square in parallel with the ring.

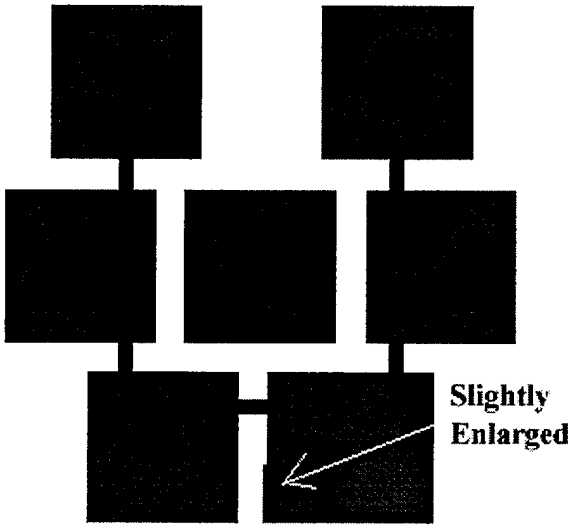

Figure 6. 5 Capacitor layout geometry. From [Ref. 22, p. 48]

C. THE LINEAR ACCELERATOR

The source of radiation which provided the ionizing damage to the capacitors was the Naval Postgraduate School Linear Accelerator (LINAC). It consists of three 22 Megawatt (peak) klystrons amplifiers, each powering a ten foot accelerator section. A diagram illustrating the major components of the LINAC can be seen in Figure 6.6. An electron gun injects 80 keV electrons into the accelerator sections and the electrons are modulated into packets by the klystrons. The frequency and pulse width of the electron beam is 60 Hz and 3.5 μsec, respectively. Following the third accelerator section is a

collimator which provides a source point for the deflection magnet and quadrapole lenses, used to steer the beam at the target. [Ref. 24, p. 41]

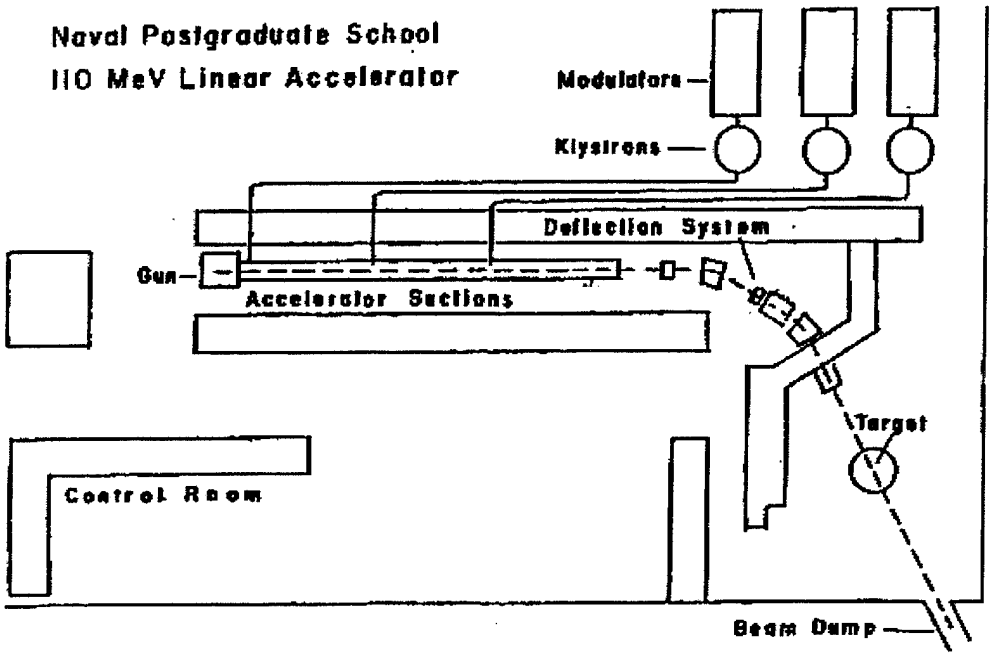

Figure 6. 6 The NPS Linear Accelerator. From [Ref. 25, p. 73]

The LINAC employs a secondary emissions monitor (SEM) at the end of the target chamber. It measures the total fluence of electrons passing through the target. The SEM is simply a charge accumulator. As electrons pass through it, charge accumulates over time on a variable capacitor whose value is selected in the control room before the irradiation is performed. A voltage, V, is then derived from

$$V = Nq = \frac{Q}{C} \qquad \textbf{(6. 2)}$$

where

N = Number of electrons
q = Charge of an electron
Q = Total charge accumulated
C = Variable capacitance selected in control room

Therefore, given a desired electron fluence or total charge per area, Q, similar to that experienced by a spacecraft in orbit, one can use Equation 6.2 to calculate the voltage needed to be produced by the LINAC. It is important to note that the SEM is only 10% efficient. This fact must be incorporated into calculations using Equation 6.2 in order to arrive at the correct total fluence.

D. EXPERIMENTAL DESCRIPTION

1. Construction of the Low Pass Filters

The first circuits were constructed using an CTI SB-147 Experimental Board. This board has rails of metal used for interconnections underneath plastic pegboard. Since the filters had extremely low capacitance values, some concern was given to the amount of stray capacitance that could be contributed to the filters by the board. To solve this issue, new circuits were constructed on plastic pegboard using wire-wrap connections only where necessary, eliminating any extraneous metal and reducing stray capacitance. The 40 pin chip containing the capacitor was connected to the circuit via a low insertion force chip socket. This allowed a target MOSIS chip to be irradiated, measured and then easily replaced with another IC for more tests.

2. Frequency Measurement and Capacitance Calculation

To stimulate and measure the filters, a Hewlett-Packard 3585B Signal Generator/Spectrum Analyzer was used. The signal generator was set to sweep the low pass filters from 250 Hz to 50 kHz. The scope displayed the gain in decibels as a function of frequency. The frequency corresponding to a 3dB drop in gain was used in

Equation 6.1 to calculate the pre-irradiation values of capacitance. Next, each chip was subjected to electron bombardment in the LINAC. The results are discussed in Chapter VII.

VII. RESULTS

Each filter was measured to find the pre-irradiation corner frequency, which allowed an initial capacitance value to be calculated using Equation 6.1. Unfortunately, due to a design error or manufacturing flaw, the center/ring capacitor set which is pictured in the lower left corner of Figure 6.2 was inoperable. This left the experiment with only three operational amplifiers per MOSIS chip.

Given the estimated 3.5-14 pF capacitance range, resistors for the filters were selected to provide a closed loop gain of 10 and a target corner frequency of 10 kHz. A representative low pass filter output as recorded by the 3585B signal generator/spectrum analyzer is shown in Figure 7.1. This particular plot was generated using chip HG2 #1, capacitor #1.

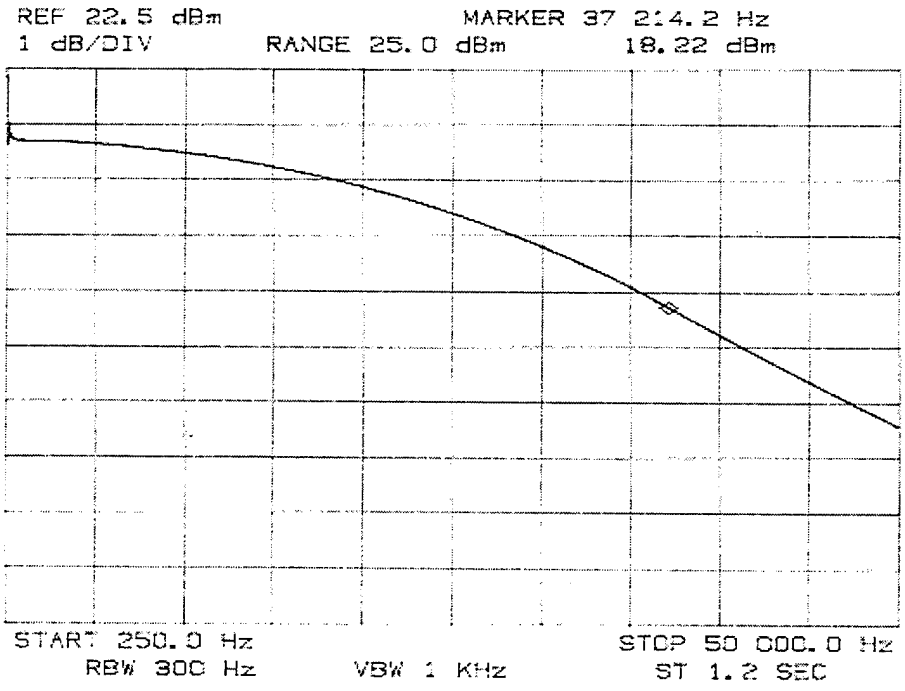

Figure 7. 1 Baseline pre-LINAC low pass filter output.

A. ADAPTATION TO THE LINAC

The LINAC has an extremely high electrical noise environment. To combat this problem, 50 Ω coaxial cables shielded with copper run the entire length of the accelerator from the target chamber to the control room and are available for experimental insulation. Four coaxial BNC connectors (one for the input signal and one for each remaining filter output signal) were constructed and attached to the circuit board. The circuit board was placed in the target chamber between the end of the electron waveguide and the SEM, shown in Figure 7.2. Television cameras were aimed at the chip for monitoring purposes discussed below. The circuits were tested again for proper function in both an innocuous and a non-benign noise environment. Filter outputs were measured with and without the klystrons operating but always without electron beam firing. Resulting plots using HG2 #1, capacitor #1, are shown in Figure 7.3 and Figure 7.4. The new modification to the board performed well. There is admittedly some noise in the plots, especially at the lower frequencies, but the overall shape, gain and break frequency remained nearly the same. The sinusoidal noise appeared to lessen slightly with the klystrons on.

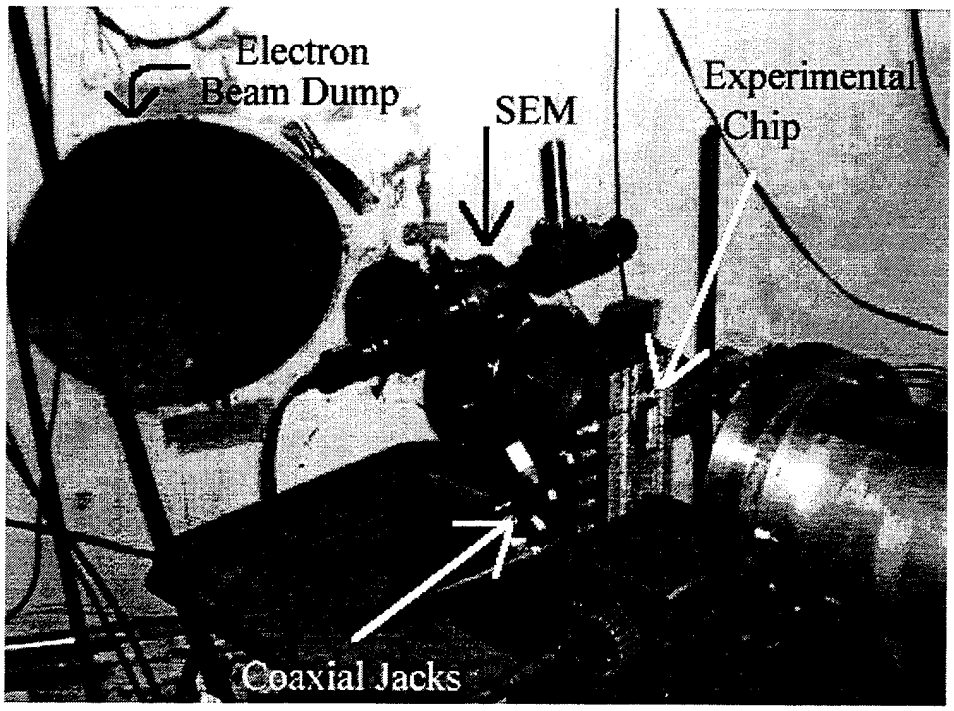

Figure 7. 2 Photograph of circuit placement in the LINAC target chamber.

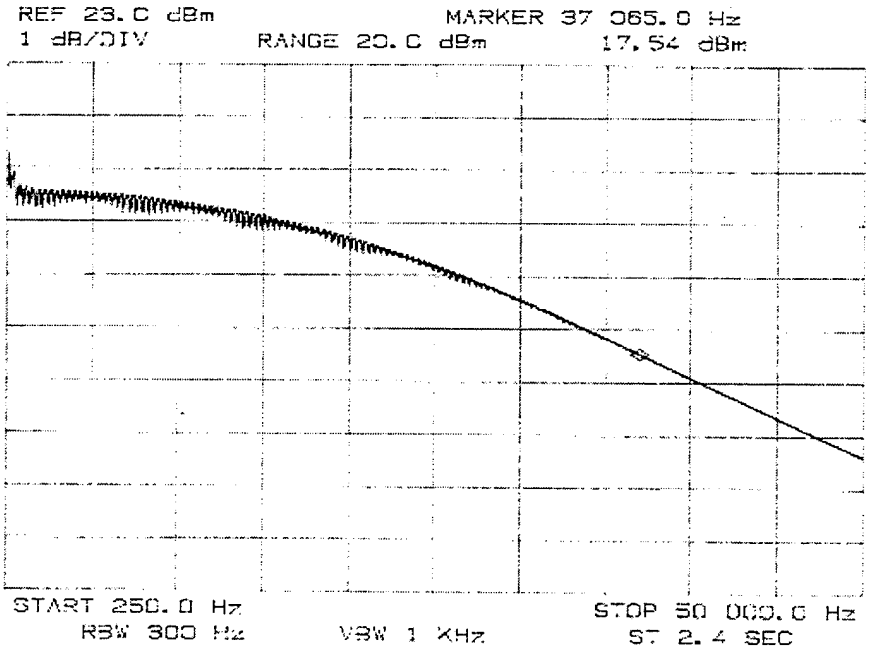

Figure 7. 3 LINAC modification plot without klystron interference.

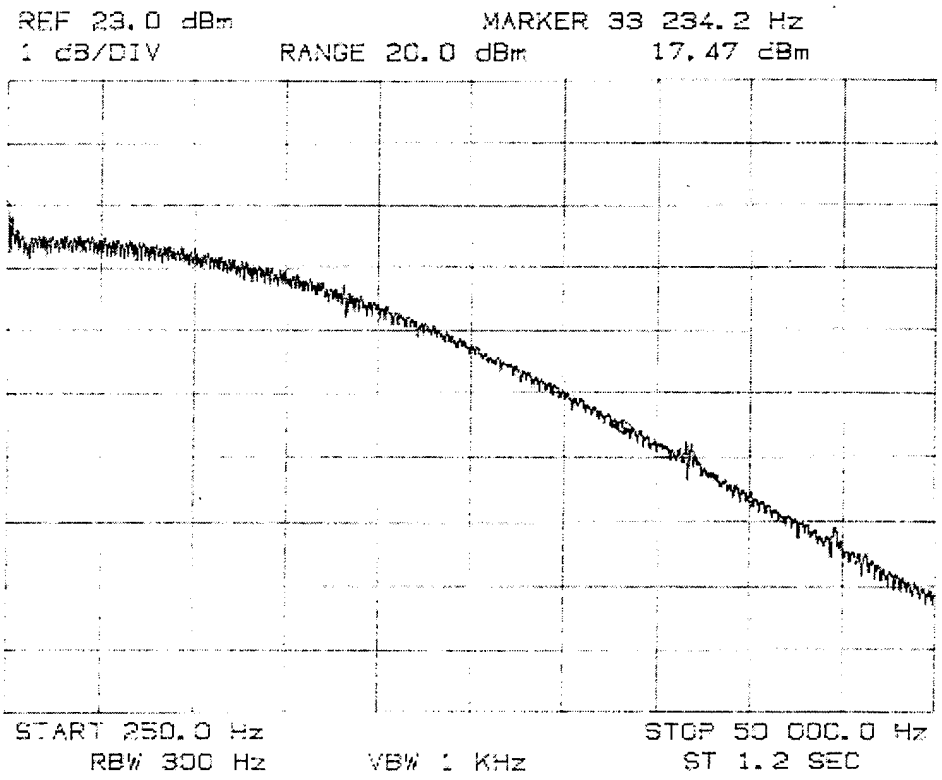

Figure 7. 4 LINAC modification plot with klystron interference.

B. IRRADIATION #1

The first irradiation involved chip HG2 #1 on 18 October 1995. Since these were the first in situ experiments of this type, there was uncertainty as to choosing the proper irradiation dose for the capacitors. A reasonably attainable fluence in space of $1x10^{15}$ electrons/cm^2 was chosen to be the target for the first experiment. Using the SEM as a fluence counter and converting numbers of electrons per area to desired charge by

$$Q_{desired} = N_{e^-} * K * \mu_{SEM} \qquad (7.1)$$

where

N_{e^-} = number of electrons/cm^2
$K = 6.25x10^{-20}$ Coulombs/electron (conversion factor)
$\mu_{SEM} = 0.10$ ➔ SEM efficiency

This resulted in $Q_{desired}$ = 6.25x10^{-6} Coulombs. The variable capacitor in the control room was set to 1 μF. Using Equation 6.2, the integrated amount of charge or voltage required was 6.25 V.

In order to steer the beam onto the chip and to ensure that it is receiving the center of the electron beam, electroluminescent tape was applied to the outer surface of the chip with a cross for beam alignment drawn directly over the center of the chip. When the beam is turned on, it excites electrons in the tape into the conduction band and as they fall back into the valence band, they emit photons which are seen as light. See Figure 7.5. The beam now may be monitored and aimed via a closed circuit television set in the control room. The electron beam is considered to have uniform flux across the cross section for the entire chip.

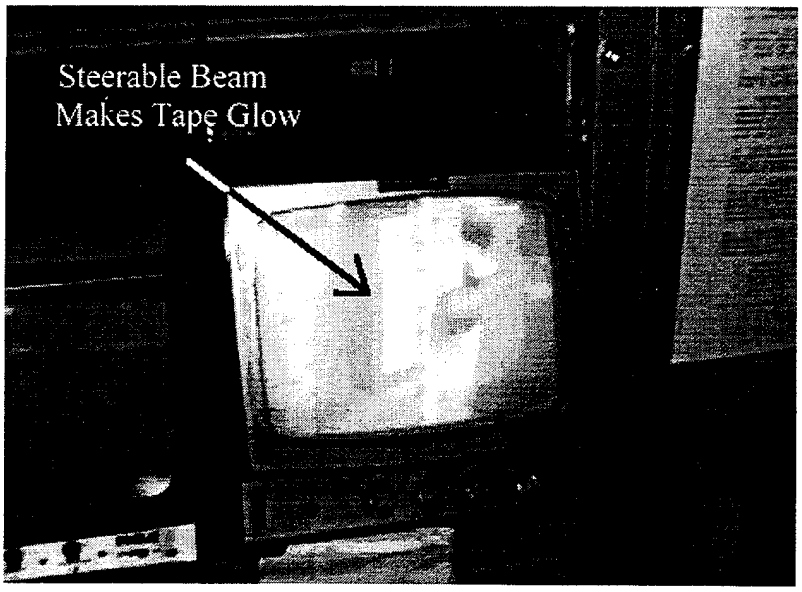

Figure 7. 5 MOSIS chip glowing under irradiation.

Measured baseline values for all components of each filter are provided in Figures 7.6 and 7.7. Notice the capacitance values are all well within Silvernagel's predicted

range of 0.5-14.0 pF. HG2 #4 was never measured in the LINAC with the environmental noise and shielded cables. The values for this chip are taken from the laboratory where the circuit board was constructed which has a less intrusive noise environment. Also worthy of noting is the fact that capacitor #4 on each chip had an average of 35.9% higher values of capacitance. The reason for this is as yet unknown. One speculation is a manufacturing or specification error as with capacitor #3.

The electron beam was turned on at time 1115. The LINAC provided electrons this day with energies of 26 MeV. Amplifier circuit #1 and #2 failed at 1116:05 or just after one minute and immediately after the first reading for amplifier #4 was taken. On average, it takes 15-20 seconds to measure and record each amplifier gain and frequency, which, with 3 amps per chip, allows a complete chip measurement every minute. The failure was extremely rapid and no sign of degradation was evident until actual failure. No picture was recorded due to the speed of failure but a visual verification of both the gain and corner frequency decrease occurred, which supports the research hypothesis.

An interesting phenomenon was observed with amplifier #4, however. Upon commencement of radiation, the corner frequency climbed rapidly while the gain decreased. Then, as irradiation continued, the corner frequency decreased and reached a stabilized point near the baseline measurement. The gain also seemed to stabilize at approximately the baseline value. Table 7.1 shows the 3_{dB} frequency and gain with the corresponding irradiation time. The total fluence, according to Equation 6.2, was 1.44×10^{15} electrons/cm^2, which is a viable number in the natural space environment.

Test Data
Chip ISI N3AB HG2 #1

17 Oct 95

Op Amp n		Resistances R_0 (MΩ)	Resistances R_1 (kΩ)	Frequency (Hz) 3 db cutoff	Gain (dbm) Initial	Gain (dbm) -3 dbm
1		0.993	99.500	33234.2	21.22	18.22
2		0.970	99.100	33085.0	21.14	18.14
3	INOP	1.037	99.000	-	-	-
4		1.024	99.300	22985.7	21.50	18.50

Capacitance Calculation

using	Capacitor	$C_{measured}$ (pF)
$f=1/2\pi R_oC$:	1	4.82
	2	4.96
	3	N/A
	4	6.76

Test Data
Chip ISI N3AB HG2 #2

18 Oct 95

Op Amp n		Resistances R_0 (MΩ)	Resistances R_1 (kΩ)	Frequency (Hz) 3 db cutoff	Gain (dbm) Initial	Gain (dbm) -3 dbm
1		0.993	99.500	34975.5	21.24	18.24
2		0.970	99.100	34378.5	21.16	18.16
3	INOP	1.037	99.000	-	-	-
4		1.024	99.300	23732	21.50	18.50

Capacitance Calculation

using	Capacitor	$C_{measured}$ (pF)
$f=1/2\pi R_oC$:	1	4.58
	2	4.77
	3	N/A
	4	6.55

Figure 7. 6 Capacitors #1-2 baseline values.

Test Data — 18 Oct 95

Chip ISI N3AB HG2 #3

Op Amp n		Resistances R_0 (MΩ)	Resistances R_1 (kΩ)	Frequency (Hz) 3 db cutoff	Gain (dbm) Initial	Gain (dbm) -3 dbm
1		0.993	99.500	34328.7	21.25	18.25
2		0.970	99.100	33682.0	21.14	18.14
3	INOP	1.037	99.000	-	-	-
4		1.024	99.300	24329.0	21.53	18.53

Capacitance Calculation		Capacitor	$C_{measured}$ (pF)
using	$f=1/2\pi R_0 C$:	1	4.67
		2	4.87
		3	N/A
		4	6.39

Test Data — 11 Oct 95

Chip ISI N3AB HG2 #4

Op Amp n		Resistances R_0 (MΩ)	Resistances R_1 (kΩ)	Frequency (Hz) 3 db cutoff	Gain (dbm) Initial	Gain (dbm) -3 dbm
1		0.993	99.500	37114.7	21.24	18.24
2		0.970	99.100	37264.0	21.16	18.16
3	INOP	1.037	99.000	-	-	-
4		1.024	99.300	27164.7	21.55	18.55

Capacitance Calculation		Capacitor	$C_{measured}$ (pF)
using	$f=1/2\pi R_0 C$:	1	4.32
		2	4.40
		3	N/A
		4	5.72

Figure 7. 7 Capacitors #1-2 baseline values.

TIME (min)	Filter #4 3 dB Frequency (Hz)	Gain (dBm)
Baseline	22985.7	17.80
3	29403.5	16.64
6	28508.0	16.70
9	27861.2	16.95
10	26468.2	17.22
12	24975.7	17.44
14	25174.0	17.48
16	24378.7	17.70
18	23980.7	17.74
20	24229.0	17.70
22	24229.5	17.70
24	24229.5	17.70
26	24080.2	17.70
28	24179.2	17.72
30	24179.7	17.70
32	24080.0	17.76

Table 7. 1 HG2 #1 amplifier #4 irradiation results.

C. IRRADIATION #2

Upon examining the circuit after radioactive cooling had taken place, it was discovered that the circuit had heated during the irradiation process and had actually discolored the pegboard. In order to monitor the temperature of the chip during the next experiment, a thermocouple was placed in between the chip and the low insertion force socket. Another video camera was placed in the target chamber enabling temperature display in the control room, as seen in Figure 7.8.

Figure 7. 8 Temperature display in control room via video.

In an effort to make the first two filters last longer, it was decided to lower the fluence by an order of magnitude. A target fluence of $1x10^{14}$ e^-/cm^2 was selected for HG2 #2 on 18 October 1995. This required a total voltage of 0.625 V in the control room charge integrator, again using 1 μF or the variable capacitor setting. Table 7.2 reports these results for amplifier #4. Again, in under three minutes, both filter one and filter two, utilizing capacitor #1 and #2 respectively, failed.

TIME (min)	Temperature (°C)	Filter #4 3 dB Frequency (Hz)	Gain (dBm)
Baseline	32.1	23732.0	17.82
3	40.0	24826.0	17.46
5	42.7	24721.0	17.79
7	46.4	24470.0	17.85

Table 7. 2 HG2 #2 amplifier #4 irradiation results.

A steady climb in the temperature can be witnessed. The irradiation was stopped after 7 minutes due to two reasons. First, the failure of filters #1 and #2 and combined with the prior performance of filter #4, which stabilized during the first run and had already stabilized in the second. Second, the temperature was steadily climbing so the experiment was stopped to preclude further damage to the circuit. The total voltage on the charge integrator was 0.4 V, corresponding to a fluence of 6.4×10^{13} electrons/cm^2.

D. IRRADIATION #3

In a final effort to measure and capture the degradation of either HG2 #3 filter #1 or #2, the LINAC was tasked to fire electrons at the lowest possible rate. Another order of magnitude lower fluence was requested, but given the aged monitoring equipment in LINAC, it was not positively determined what the initial flux setting was. That is, it might have been ten times less than the second run or it might have been eight or six. The variable capacitor value for this run was 0.1 μF. Another uncertainty with this run was, the electroluminescent tape did not glow under the low electron flux. Therefore, extreme care was taken to ensure the experimental setup and alignment was not disturbed when switching HG2 #2 with HG2 #3.

During this run, filters #1 and #2 both managed to operate for 30 minutes with reduced flux. As a matter of fact, there was no noticeable degradation to any of the three amplifiers. After 30 minutes, total fluence was 8×10^{12} electrons/cm^2 and the flux was doubled. For ten minutes the flux was kept at this level and still no degradation was observed. The decision to double again was made and for eight minutes, no observable degradation occurred. Then, during a measurement of amplifier #1, a rapid failure

transpired. This time, a recording of the failure, displayed in Figure 7.9 as both a digital picture and a printout, was achieved by the Hewlett-Packard 3585B. The top curve is the baseline measurement of HG2 #3 amplifier #1. The bottom curve clearly depicts the low pass filter failure and gain-bandwidth lowering after 48 minutes under irradiation. The total voltage on the charge integrator was 1.30 V, corresponding to a fluence of 2.08 $x10^{13}$ electrons/cm^2. Table 7.3 displays the results for experiment three.

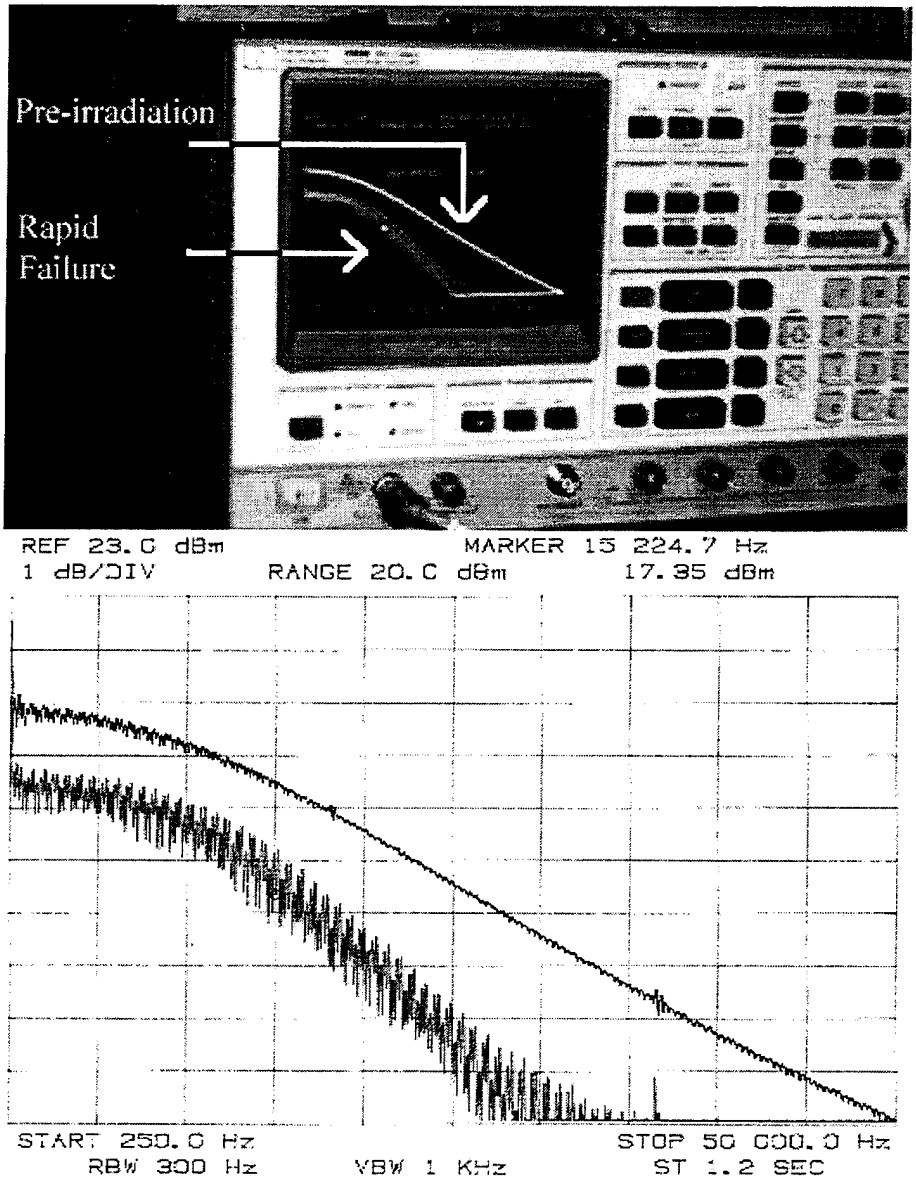

Figure 7. 9 Failure of HG2 #3 amplifier #1.

TIME (min)	Temperature (°C)	Filter #1 (3 dB)	Filter #2 (3 dB)	Filter #4 (3 dB)	Gain #1 (dBm)	Gain #2 (dBm)	Gain #4 (dBm)
Baseline	89.0	34328.7	33682.0	24329.0	17.5	17.45	17.75
1	89.4	34975.0	33682.0	N/A	17.4	17.35	N/A
2	90.5	34527.0	34030.0	23284.0	17.47	17.33	17.9
3	91.4	34925.0	34030.0	23980.0	17.4	17.32	17.76
5	92.4	34129.0	34080.0	23831.0	17.49	17.35	17.77
8	92.8	34378.0	34079.0	24080.0	17.44	17.35	17.77
12	93.3	34279.0	33930.0	23732.0	17.44	17.32	17.79
15	93.5	34627.0	34030.0	23980.0	17.43	17.35	17.79
20	93.5	34527.0	33881.0	23732.0	17.45	17.35	17.81
25	93.2	34080.0	33179.0	23682.0	17.46	17.32	17.81
30	90.8	34478.0	33930.0	23831.0	17.4	17.35	17.79
FLUX	DOUBLED						
35	89.5	34338.0	34030.0	23881.0	17.45	17.35	17.78
40	89.5	34428.0	34279.0	24030.0	17.45	17.31	17.76
FLUX	DOUBLED						
48	90.8	FAILED	FAILED	N/A	N/A	N/A	N/A

Table 7. 3 HG2 #3 amplifier #1,2 & 4 irradiation results.

VIII. CONCLUSIONS AND RECOMMENDATIONS

This research intended to investigate the effects of radiation on parallel plate MOS capacitors. Previous work had suggested performance of a low pass filter would increase due to radiation received over a lifetime in orbit. This was counterintuitive and a novel experiment was performed to validate the hypothesis of degraded filter operations resulting from electron irradiation.

The anticipated results of irradiating the elementary low pass filters confirmed expectations. The corner frequency indeed lowered as the capacitor received larger and larger doses of radiation. The problem is they failed too fast for analysis. They gave no warning of impending failure while irradiated with 26 MeV electrons with the LINAC.

After the experiment of HG2 #3, resistance measurements were performed on each individual capacitor by connecting a hand-held ohmmeter to the corresponding pin-outs as seen in Figure 6.2. It is interesting to note that after irradiation, capacitors #1 and #2, which failed, had finite resistance values. This suggests the radiation might have actually changed the conductive properties of the capacitor. More specifically, the oxide layer probably developed a plethora of trapped charges thus changing the oxide from an insulator to more of a conductor. This ultimately caused the capacitors to short-circuit and is the suspected failure mechanism of the low pass filters. The relatively radiation tolerant performance of capacitor #4 on each chip is physically unexplainable in this effort. One hypothesis is that if it were exposed to further radiative sources, it would eventually fail due to the same mechanisms as #1 and #2.

The MOSIS chips are known to be radiation intolerant. This fact was known before this research was started. However, the HG2 series chips were the only integrated circuits available for this experiment, possessing accessible parallel plate MOS capacitors.

This experiment should serve as a baseline for further studies. Future work in this area include the following suggestions: Use the VLSI Design class (EC 4870) to construct numerous IC chips containing solely MOS/CMOS parallel plate capacitors. This would serve to eliminate some of the uncertainty of this experiment, specifically, probable stray capacitance and failure within the op amp compensating capacitors either due to design flaw (recall the malfunctioning two phase non-overlapping clock), manufacturing error or both. Next, all experiments should incorporate a reliable method to calculate total dose received in the target material. A reasonable suggestion is the use of a Thermoluminescent Dosimeter (TLD). The TLD was inoperable for this experiment otherwise it would have been included. It is therefore extremely difficult, if not impossible to determine the actual dose received in the capacitance material. The SEM is neither an efficient or a reliable method. Third, the experiment proved that dose rate is definitely a factor in circuit degradation. Uncertainties with the aging linear accelerator serve to create variations in electron dose and flux from experiment to experiment. Dose rate determination can only be accomplished after the irradiation session is complete by computing total charge over time measured by a stopwatch. Along the same lines, the LINAC has a limited energy range of the particles delivered. As previously discussed, chips constructed via the MOSIS technique are not radiation tolerant and 26 MeV electrons are probably too energetic for the target material used. If the above suggested

capacitors are constructed using this technique, a solution might be to use another source of radiation, such as the Brookhaven Laboratory or the University of California at Davis facility where electrons on the order of 1 MeV can be created. Often, government agencies schedule linear accelerators and either do not use the facilities at all or use them sparingly. An attempt to 'piggy-back' on one of these agencies scheduled periods might prove to be a viable and cost effective solution.

LIST OF REFERENCES

1. Tabbert, C., "A Historical Perspective," *Space Product News*, Harris Semiconductor, Melbourne, FL, September, 1993.

2. Heinz, O., Olsen, R. C., "Introduction to the Space Environment," Physics 2514 Course Notes, Naval Postgraduate School, Monterey, CA, 1993.

3. Corliss, W. R., *Space Radiation*, United States Atomic Energy Commission Office of Information Services, 1968.

4. Stassinopoulos, E. G., Raymond, J. P., "The Space Radiation Environment for Electronics," *Proceedings of the IEEE*, Vol. 76, No. 11, November, 1988.

5. Schwank, J. R., *Basic Mechanisms of Radiation Effects in the Natural Space Radiation Environment*, Sandia National Laboratories, Albuquerque, NM, July, 1994.

6. Ricketts, L. W., *Fundamentals of Nuclear Hardening of Electronic Equipment*, John Wiley & Sons, Inc., New York, NY, 1972.

7. Adams, Jr., J. H., Silberberg, R., Tsao, C.H., "Cosmic Ray Effects on Microelectronics, Part I: The Near Earth Particle Environment," *NRL Memorandum Report 4506*, August 25, 1981.

8. Messenger, G. C., Ash, M. S., *The Effects of Radiation on Electronic Systems, 2nd ed.*, Van Nostrand Reinhold, New York, NY, 1992.

9. Sawyer, D. M., Vette, J.I., "AP8 trapped proton environment for solar maximum and solar minimum," *Rep. NSSDC 76-06*, National Space Science Data Center, Greenbelt, MD, December, 1976.

10. Sze, S.M., *Semiconductor Devices, Physics and Technology*, John Wiley & Sons, Inc., New York, NY, 1985.

11. Grebene, A. B., *Bipolar and MOS Analog Integrated Circuit Design*, John Wiley & Sons, Inc., New York, NY, 1984.

12. Blicher, A., *Field-Effect and Bipolar Power Transistor Physics*, Academic Press, Inc., New York, NY, 1981.

13. Deal, B. E., "Standardized Terminology for Oxide Charge Associated with Thermally Oxidized Silicon," IEEE Transactions of Electronic Devices, ED-27, 1980.

14. Nicollian, E. H., Brews, J. R., *MOS (Metal Oxide Semiconductor) Physics and Technology,* John Wiley & Sons, Inc., New York, NY, 1982.

15. Fleetwood, D. M., Winokour, P. S., Beegle, R. W., Dressendorfer, P. V., Draper, B. L., "Accounting for Dose-Enhancement Effects with CMOS Transistors," *IEEE Transactions on Nuclear Science*, Vol. NS-32, 1985.

16. Bourgoin, J., Lannoo, M., "Point Defects in Semiconductors II: Experimental Aspects," *Springer Series in Solid State Sciences*, Vol. 35, edited by Cardona, M., Fulde, P. and Queisser, H. J., Springer-Verlag, New York, NY, 1983.

17. Summers, G. P., "Displacement Damage: Mechanisms and Measurements," *1992 IEEE Nuclear Space and Radiation Effects Conference Short Course*, New Orleans, Louisiana, July, 1992.

18. Srour, J. R., McGarrity, J. M., "Radiation Effects on Microelectronics in Space," *Proceedings of the IEEE*, Vol. 76, No. 11, November, 1988.

19. Fleetwood, D. M., Winokour, P. S., Reber, Jr., R. A., Meisenheimer, T. L., Schwank, J. R., Shaneyfelt, M. R., Riewe, L. C., "Effects of Oxide Traps, Interface Traps and 'Border Traps' On Metal-Oxide-Semiconductor Devices," *Journal of Applied Physics*, Vol. 73, No. 10, 15 May 1993.

20. Winokour, P. S., Schwank, J. R., McWhorter, P. J., Dressendorfer, P. V., Turpin, D. C., "Correlating the Radiation Response of MOS Capacitors and Transistors," *IEEE Transactions on Nuclear Science*, Vol. NS-31, No. 6, December, 1984.

21. Michael, S. N., "Introduction to Analog VLSI," Electrical and Computer Engineering 4220 Course Notes, Naval Postgraduate School, Monterey, CA, 1994.

22. Silvernagel, G. A., "*VLSI Implementation of Stray Insensitive Switched Capacitor Composite Operational Amplifiers*," Master's Thesis, Naval Postgraduate School, Monterey, CA, December, 1993.

23. Bingham, E. W., "*Stray Insensitive Switched Capacitor Composite Operational Amplifiers*," Master's Thesis, Naval Postgraduate School, Monterey, CA, March, 1993.

24. Brittain, Jr., D. R., "*Total Dose Radiation Effects on Hardened SOI Bipolar Transistors Using the NPS LINAC*," Master's Thesis, Naval Postgraduate School, Monterey, CA, March, 1995.

25. O'Reilly, P. J., "*Effects of 30 MeV Electron Irradiation on InGaAsP LEDs and InGaAs Photodiodes*," Master's Thesis, Naval Postgraduate School, Monterey, CA, June, 1986.

INITIAL DISTRIBUTION LIST

		No. Copies
1.	Defense Technical Information Center 8725 John J. Kingman Rd., STE 0944 Ft. Belvoir, VA 22060-6218	2
2.	Library, Code 013 Naval Postgraduate School Monterey, CA 93943-5101	2
3.	Chairman, Code EC Department of Electrical and Computer Engineering Naval Postgraduate School Monterey, CA 93943-5121	1
4.	Chairman, Code AA Department of Aeronautical and Astronautical Engineering Naval Postgraduate School Monterey, CA 93943-5106	1
5.	Professor Sherif Michael, Code EC/Mi Department of Electrical and Computer Engineering Naval Postgraduate School Monterey, CA 93943-5121	4
6.	Professor Oscar Biblarz, Code AA/Bi Department of Aeronautical and Astronautical Engineering Naval Postgraduate School Monterey, CA 93943-5106	1
7.	COMMANDER CARRIER GROUP TWO ICO COMNAVAIRLANT Attn: Lieutenant Stuart M. Abrahamson Naval Air Station Norfolk, VA 23511	1